

# Destabilization of buried carbon under changing moisture regimes

Manisha Dolui<sup>1†</sup>, Teneille Nel<sup>1\*†</sup>, Abbygail R. McMurtry<sup>2</sup>,  
Stephanie Chacon<sup>1</sup>, Joseph A. Mason<sup>3</sup>, Laura M. Phillips<sup>2</sup>,  
Erika Marin-Spiotta<sup>3</sup>, Marie-Anne de Graaff<sup>2</sup>,  
Asmeret Asefaw Berhe<sup>1</sup>, Teamrat A. Ghezzehei<sup>1</sup>

<sup>1</sup>\*Department of Life and Environmental Sciences, University of  
California, Merced, 5200 Lake Rd, Merced, California, 95343, United  
States.

<sup>2</sup>Department of Geography, University of Wisconsin-Madison, 550  
North Park Street, Madison, Wisconsin, 53706, United States.

<sup>3</sup>Department of Biological Sciences, Boise State University, 1910  
University Drive, Boise, Idaho, 83725, United States.

\*Corresponding author(s). E-mail(s): [teneille.nel@gmail.com](mailto:teneille.nel@gmail.com);

†These authors contributed equally to this work.

## Abstract

Paleosols formed by the burial of topsoil during landscape evolution can sequester substantial amounts of soil organic carbon (SOC) over millennia due to protection from surface disturbances. We investigated the moisture sensitivity of buried SOC storage in the Brady paleosol, a loess-derived soil in Nebraska, USA, where historical aeolian deposition during the Pleistocene–Holocene transition buried soils up to 6 m deep. Topsoils from erosional (up to 1.8 m depth) and burial (up to 5.8 m depth) transects were incubated under two moisture regimes - continuous wetting (60% water-holding capacity) and repeated drying–rewetting - to assess soil organic matter (SOM) vulnerability to changing hydrologic conditions. SOC decomposition rates modeled from CO<sub>2</sub> fluxes were consistently higher in erosional than burial settings, with surface re-exposure of Brady soils enhancing microbial accessibility and destabilization. A two-pool model showed that >96% of SOC was stored in a slow-cycling pool, particularly in deeply buried soils where stabilization was linked to mineral association, fine particles, and Ca-mediated flocculation. However, this pool decomposed more rapidly in shallower Brady

001  
002  
003  
004  
005  
006  
007  
008  
009  
010  
011  
012  
013  
014  
015  
016  
017  
018  
019  
020  
021  
022  
023  
024  
025  
026  
027  
028  
029  
030  
031  
032  
033  
034  
035  
036  
037  
038  
039  
040  
041  
042  
043  
044  
045  
046

047 soils (higher turnover rate relative to buried soil), reflecting increased microbial  
048 responsiveness to surface-driven processes.  
049 Drying–rewetting cycles caused greater C losses from Brady soils than continuous  
050 wetting, despite the dominance of the slow pool and depletion of labile C. These  
051 cycles also accelerated fast pool decay in modern soils and erosional transects,  
052 whereas burial dampened variability in Brady soils. Although continuous wetting  
053 increased overall decay in burial transects during the incubation period, wet–dry  
054 cycles destabilized the slow pool, which may result in greater long-term C loss.  
055 Together, these results underscore the importance of burial depth, geomorphic  
056 context, and moisture regime in shaping the long-term vulnerability of ancient  
057 SOC under climate change.

058 **Keywords:** paleosol, erosion, soil carbon stabilization, organic matter decomposition

059

060

061

## 062 1 Introduction

063

064 Global temperatures have risen by 1°C since the industrial era due to anthropogenic  
065 CO<sub>2</sub> emissions, confirming human-driven climate change (IPCC, 2018). Alongside  
066 warming, precipitation regimes are shifting - marked by increased frequency and  
067 intensity of wetting and drying events, especially in more arid ecosystems. These  
068 hydrologic fluctuations can destabilize long-stored soil organic carbon (SOC) by  
069 disrupting aggregates, increasing dissolution and solute mobility, and stimulating  
070 microbial decomposition (Berhe et al., 2012; Min et al., 2020; Hicks Pries et al.,  
071 2023). While limiting warming to below 2°C remains critical, mitigation via emissions  
072 reductions alone may be insufficient. Preserving or enhancing terrestrial carbon sinks,  
073 especially soils, offers a complementary pathway for climate stabilization.

074 Soil organic matter (SOM) encompasses the full suite of organic compounds in soil,  
075 including living biomass, particulate debris, and mineral-associated organic molecules.  
076 SOC refers specifically to the carbon fraction of SOM and is the metric used through-  
077 out this study to quantify carbon stocks and fluxes. While many studies examine  
078 topsoil carbon dynamics, whole-soil responses to changes in climate have rarely been  
079 tested (Hicks Pries et al., 2017). Subsoils hold nearly half of global SOC stocks (Job-  
080 bagy and Jackson, 2000) and this deep-soil carbon may be more sensitive to varying  
081 environmental conditions than surface soil (Min et al., 2020). Organic inputs reach  
082 subsoils via leaching of dissolved organic carbon and vertical transport of litter by  
083 bioturbation. SOC in deeper horizons typically features low carbon to nitrogen (C:N)  
084 ratios and long mean residence times, suggesting advanced microbial processing and  
085 relative stability (Rumpel and Kögel-Knabner, 2011). In contrast, topsoils buried by  
086 aeolian or alluvial deposition often retain legacy carbon signatures reflecting past veg-  
087 etation and climate (Marin-Spiotta et al., 2014), diverging from modern surface soils.  
088 These buried soils have historically been isolated from near-surface conditions, includ-  
089 ing temperature and moisture fluctuations. Previous research supports this isolation  
090 effect: for instance, Chaopricha (2013) found negligible CO<sub>2</sub> fluxes from Brady Soil  
091 collected from 4 m below the modern surface when no water was added, indicating  
092 extremely limited microbial activity under such dry, oxygen-poor conditions.

The stability of buried SOC, however, depends entirely on continued isolation from surface conditions – an assumption increasingly at odds with landscape dynamics across the Great Plains. Accelerated gully erosion, agricultural tillage, and more intense precipitation events are progressively exhuming paleosols that remained protected for millennia (Mason et al., 2008; Jacobs and Mason, 2007; Thaler et al., 2021). Yet the decomposition response of this ancient carbon to re-exposure remains poorly constrained. Will millennia-old SOC decompose rapidly once oxygen and moisture access is restored, or do the same properties that enabled its long-term preservation – fine texture, mineral associations, chemical recalcitrance – confer lasting resistance? This uncertainty carries substantial implications for carbon-climate feedbacks: if re-exposed paleosol carbon proves vulnerable to decomposition, ongoing erosion across loess landscapes could convert a long-term carbon sink into an unaccounted source.

Subsurface environments typically have limited oxygen, C inputs, and water availability, all of which constrain microbial activity and promote long-term SOC persistence (Soong et al., 2021). However, this protection may be compromised under climate change scenarios involving increased rainfall, warming, and surface disturbance (Fontaine et al., 2007; Gao et al., 2020; Hicks Pries et al., 2023). While burial isolates SOM from decomposers, enhancing its stability (Berhe et al., 2007; Stacy et al., 2015; Berhe et al., 2008), soil erosion, root intrusion, and hydrologic shifts can re-expose previously protected SOM. While erosion may remove C, the exposure of fresh relatively unweathered parent material can increase photosynthate additions due to the rejuvenation of rock-derived nutrients (Berhe et al., 2018). Given the global extent of geomorphic disturbance and the potential for reactivated decomposition, buried soils may represent an extensive but under-characterized carbon pool whose long-term persistence is uncertain (Chaopricha and Marín-Spiotta, 2014; Szymanski, 2021; Pal et al., 2023).

SOM decomposition is mediated by geomorphic and geochemical controls. Soil texture, mineralogy, and ionic composition regulate organo–mineral associations and microbial accessibility. Mineral surfaces – particularly clays and metal oxides – can stabilize SOM through sorption and aggregation, while spatial inaccessibility and microsite heterogeneity further constrain decomposition (Marin-Spiotta et al., 2011; Schmidt et al., 2011; Lawrence et al., 2015). Thermal transformation of buried SOM into condensed aromatic compounds can also enhance resistance to decay. Recent findings from Dolui et al. (2026b) link persistent SOM turnover in buried soils to fine textures, higher conductivity, and strengthened organo–mineral bonding, consistent with evidence that mineral-associated and physically protected pools dominate long-term persistence (Slessarev et al., 2022). However, these stabilizing mechanisms weaken with erosional exposure, as disruption of aggregates, increased oxygen availability, and shifts in moisture regimes enhance microbial activity. In addition, exposure promotes priming effects through fresh organic matter inputs, accelerating the decomposition of previously protected SOM (McMurtry et al., 2024; Lawrence et al., 2021) and increasing its vulnerability to loss.

Soil moisture dynamics are central to SOM persistence. Wetting and drying–rewetting cycles can destabilize aggregates, increase dissolved organic carbon leaching, and stimulate mineral-associated OM loss (Berhe et al., 2012; Neff and Asner,

139 2001; Li et al., 2023). Moisture influences microbial processes by modulating water  
140 potential, oxygen diffusion, and solute transport (Chowdhury et al., 2011; Davidson  
141 et al., 2012). Texture controls water retention during drying, while aggregate struc-  
142 ture governs accessibility under saturated conditions (Or and Tuller, 1999; Ghezzehei  
143 et al., 2019).

144 In surface soils, especially in semi-arid and Mediterranean systems, dry-  
145 ing–rewetting cycles produce strong mineralization pulses (Miller et al., 2005; Zhu and  
146 Cheng, 2013). Such cycles break down aggregates and release labile SOM, stimulating  
147 priming effects (Najera et al., 2020). Soils with broader pore-size distributions may  
148 retain water longer, sustaining microbial activity and potentially increasing cumula-  
149 tive SOM loss (Goebel et al., 2005). The effects of increased rainfall also depend on  
150 seasonal timing; for instance, winter precipitation can enhance subsoil C storage more  
151 than spring rain due to deeper translocation of carbon (Wahab et al., 2025).

152 As soils dry, physical and chemical processes can strengthen OM–mineral inter-  
153 actions. Solute precipitation, matric tension, and shifts toward stronger bonding  
154 (e.g., inner-sphere complexes) promote greater SOM–mineral affinity (Kaiser et al.,  
155 2015; Kemper et al., 1987; Kang and Xing, 2008). Reorientation of amphiphilic com-  
156 pounds on mineral surfaces can increase hydrophobicity (Horne and McIntosh, 2000),  
157 potentially misleading assessments of SOM stability under drier conditions.

158 CO<sub>2</sub> efflux in subsoils is shaped by physical constraints - lower porosity, higher bulk  
159 density, and greater water-filled pore space - which suppress microbial respiration after  
160 rewetting (Min et al., 2020; Hill et al., 1985; Beare et al., 2009; Schrumpf et al., 2013).  
161 Subsurface microbial communities are often dominated by drought-tolerant fungi (Bird  
162 and Torn, 2006), and experience fewer moisture and temperature fluctuations than  
163 surface soils (Rumpel and Kögel-Knabner, 2011). Microbial “resistance” to drying  
164 manifests as reduced respiration during dry-down, while “resilience” describes rapid  
165 respiration rebound after rewetting (Leizeaga et al., 2021; Griffiths and Philippot,  
166 2013). Soils with frequent drying–rewetting history tend to support more resilient  
167 microbial communities (Fierer and Schimel, 2003; Steenwerth et al., 2005).

168 In semi-arid systems, soil inorganic carbon (SIC) also contributes to carbon dynam-  
169 ics. SIC accumulates at depth through carbonate dissolution–precipitation cycles  
170 (Shariffar et al., 2023; Batoool et al., 2024; Cotrufo and Lavallee, 2025). This is seen in  
171 the Brady Soil, a late Pleistocene paleosol buried by loess ca. 13,000–10,000 years ago  
172 in the Great Plains of the US (Jacobs and Mason, 2007; McDowell, 2020). SIC inter-  
173 acts with SOC via aggregation and mineral associations but can be mobilized through  
174 leaching under increased moisture conditions (Naorem et al., 2022; Liu et al., 2018;  
175 Tsy-pin and Macpherson, 2012).

176 Despite growing interest in buried SOM, moisture-driven decomposition patterns  
177 across landforms remain unclear. This study investigates the sensitivity of modern  
178 and buried SOM to moisture inputs under erosional and burial geomorphic conditions  
179 in the Brady Soil. According to the U.S. National Climate Assessment (2018), the  
180 Central Great Plains region of Nebraska is projected to warm by 3.5–9.5°C, with  
181 annual precipitation increasing by 2.5 cm. Erosion driven by agriculture, grazing,  
182 wind, and rainfall threatens to re-expose buried SOM to surface conditions.

183  
184

We conducted a laboratory incubation using soils collected near Wauneta, Nebraska, to compare CO<sub>2</sub> efflux under continuous wetting versus drying–rewetting regimes. The area’s semi-arid climate with seasonal moisture variability provides a relevant setting to test SOM responses to hydrologic fluctuations. Our hypotheses were: (i) Brady SOM is more stable and decomposes more slowly than modern SOM as reduced moisture and oxygen availability limit decomposition of SOM due to isolation from the soil surface; (ii) buried SOM in erosional settings is more vulnerable to loss due to exposure of previously protected SOM to surface conditions and mixing with modern carbon; and (iii) wetting will stimulate CO<sub>2</sub> release from previously buried soils as a result of increased substrate availability due to enhanced dissolution, solute transport, microbial decomposition, and/or aggregate disruption. By evaluating the interactions between moisture, geomorphology, and SOM dynamics, we aim to improve predictions of carbon stability under future climate and land-use change.

## 2 Methods and materials

### 2.1 Site and sampling

The field site is situated near Wauneta, within the loess tablelands of southeastern Nebraska, USA (40°29’52.8” N, 101°24’36” W; see Fig. 1). The region experienced reduced loess input during the terminal Pleistocene and early Holocene (13–10 ka) that permitted soil formation, leading to the development of the Brady Soil. Subsequent aridification renewed dust flux, resulting in its burial by younger loess (Johnson et al., 2007; Mason et al., 2008). Additional loess accumulation throughout the Holocene preserved weaker paleosols formed during intermittent burial pauses (Mason et al., 2003; Miao et al., 2007). Recognized as a key paleoenvironmental and stratigraphic unit, the Brady Soil is regionally traceable across Nebraska, northeastern Colorado, and northern Kansas (Johnson and Willey, 2000).

The area is characterized by broad, flat uplands and sharply incised edges, providing natural windows into stratified soil profiles. Loess cover above the Brady Soil tapers in a downwind direction across the summits where it is thickest, producing burial transects of variable thickness. The local climate is semi-arid, with an average annual temperature of 9.7°C and ca. 495 mm of precipitation, concentrated during the summer months, with occasional snow in winter. Natural vegetation includes a mix of C3 and C4 grasses, replaced by cropland on many level surfaces today, but remaining at the study site and on steeper terrain in general.

Brady Soil exposures are visible in actively eroding margins, gullies, and roadside cuts. Prior investigations, including coring and field surveys, confirm its continuity beneath the summit landform (Jacobs and Mason, 2004; Marin-Spiotta et al., 2014; Mason et al., 2008). Surface soils developed in Holocene loess are weakly developed and light-colored, typically classified as Mollisols, Inceptisols, or Entisols. Although different in age, modern and buried soils share similar parent material and mineralogy due to the region’s limited weathering intensity. Brady A horizons (Ab) are identified by their dark grayish brown coloration (Munsell 10YR3/2 to 10YR4/2) and silt loam texture, generally overlying Bk or Bw horizons (Szymanski, 2021; Jacobs and Mason, 2007; McDowell, 2020).

231 Sampling was conducted in 2016 and 2017 across two geomorphic settings: burial  
232 transects (where the Brady Soil is deeply buried beneath Holocene loess) and erosional  
233 transects (where the Brady Soil is exposed or shallowly buried due to hillslope erosion).  
234 Within each setting, three replicate transects were established. We collected samples  
235 at three depths relative to the soil surface from each of the transects per setting  
236 (details in Fig. 1). Sampling stratigraphy relative to the present land surface was  
237 categorized using Roman numerals (Supplementary Information, Table A1). At each  
238 transect position, samples were collected from (1) the modern soil surface (0–30 cm),  
239 (2) the subsurface modern soil (30–60 cm, where present), and (3) the upper Brady  
240 paleosol horizon (0–30 cm into the Ab horizon, at variable depth below the modern  
241 surface depending on burial thickness). All samples were analyzed for physicochemical  
242 properties, but only samples from the 0–30 cm depth intervals were used for incubation  
243 experiments. Table A1 provides the specific sampling depths from the soil surface for  
244 each transect position. A Giddings probe (10.2 or 8.9 cm diameter) with plastic liners  
245 was used for intact sampling in burial settings, while soil pits were dug for erosional  
246 profiles. Complete methods are described in (Szymanski, 2021).

247

## 248 2.2 Soil chemical and physical analyses

249

250 General soil physical and chemical properties were determined by standard soil ana-  
251 lytical methods, as described in detail in Dolui et al. (2026b) and Szymanski (2021).  
252 Briefly, soil pH and electrical conductivity (EC) of soil samples were determined in  
253 1: 2 water extracts using a SevenExcellence multiparameter benchtop meter (Met-  
254 tler Toledo, United States). Total carbon was determined by dry combustion using  
255 an ECS 4010 elemental combustion analyzer (Costech Analytical Technologies, Inc.,  
256 USA); inorganic carbon was removed by acidification with 1M HCl prior to TOC  
257 determination. Exchangeable base cations ( $\text{Ca}^{2+}$ ,  $\text{Mg}^{2+}$ ,  $\text{Na}^{+}$  and  $\text{K}^{+}$ ) were  
258 quantified by ICP-OES (Optima 5300 DV Spectrometer, Perkin-Elmer, Germany) fol-  
259 lowing ammonium acetate extraction (buffered to pH 7). Sodium adsorption ratio  
260 (SAR) was determined by dividing concentration of Na in soil extract by the square  
261 root of half of sum of Ca and Mg concentrations (Dolui et al., 2026a). Particle size  
262 distribution was determined using the pipette method for clay ( $< 2\mu\text{m}$ ) and laser  
263 diffraction (Mastersizer 2000 particle size analyzer, Malvern Panalytical, UK) for silt  
264 and sand fractions. Radiocarbon ( $^{14}\text{C}$ ) analyses of bulk soil samples were conducted  
265 to determine the age and turnover time of carbon in both modern and buried soils.  
266 Samples were pre-treated, combusted, and then measured by accelerator mass spec-  
267 trometry using an FN accelerator mass spectrometer (Van de Graaff, US) at the  
268 center for accelerator mass spectrometry at Lawrence Livermore National Laboratory.  
269 The  $\Delta^{14}\text{C}$  results were used in a homogeneous, open-system, steady-state soil carbon  
270 decomposition model to estimate carbon turnover times (Dolui et al., 2026b) which  
271 were averaged for the three replicate transects.

272

## 273 2.3 Incubation experiments

274

275 The incubation experiment was set up to determine the effect of continuous wetting  
276 and drying–rewetting on SOC fluxes using soils that were collected from the upper

layer of modern and Brady Soil samples at burial and erosional transect types. To isolate the effects of moisture, roots >2 mm were removed by sieving and manual sorting. Samples from 0-30 cm horizon depth from different transect numbers were homogenized (so that they had only unique paleostatus, transect type and burial/ erosional degree). Two types of water addition experiments were conducted: continuous wet and drying-rewetting. Two sub-samples were taken from each composite to perform biological replicates of each incubation experiment, such that there was a total number of 24 individual incubation vessels.

### 2.3.1 Experimental setup

The incubation experiments were conducted in 8 oz mason jars. Soil water holding capacity (WHC) was pre-determined by tensiometry (using pressure plates with an applied pressure of -33 kPa) and soil moisture content was monitored on a mass-basis by weighing soils weekly during the incubation. The treatments included (i) continuous wet - soils maintained at 60% WHC throughout the experiment and (ii) drying-rewetting cycles - soils were dried, then rewetted to 60% WHC. Treatment durations differed by experimental objective. The continuous wet incubation (225 days) was designed to capture the full trajectory of decomposition, enabling robust fitting of two-pool decay models that partition SOC into fast- and slow-cycling fractions (turnover times on the scale of days and centuries, respectively). The wet-dry treatment (56 days, 8 cycles of 7-day drying followed by rewetting) was designed to assess cumulative effects of repeated moisture pulses over a timeframe comparable to a growing season. For direct comparison between treatments, we modeled CO<sub>2</sub> loss over equivalent 49-day windows and compared decay parameters derived from each treatment's full duration. Each treatment had two biological replicates (sub-samples derived from a single composite of replicate transects per soil type), and control soils were maintained at 5% WHC.

Previously homogenized soils were sub-sampled and added to jars at an equivalent of  $30 \pm 0.5$  g dry mass. After adding a predetermined amount of ultra-pure water ( $18.2 \text{ M}\Omega \cdot \text{cm}$ ), the jars were kept at room temperature (ca. 25°C), matching the average summer soil temperature (when most precipitation occurs) at the site (UNL Soil Temperature Data). Jars were sealed with lids fitted with rubber septa for headspace gas collection, and silicone gel was applied around the septa to prevent gas leakage.

In the continuous wet experiment, soils were maintained at 60% WHC and sealed until sampling. On average, water loss was 0.01 mL/day, ranging from 0.005 to 0.02 mL/day. Water was added after gas sampling to avoid inducing the Birch effect. After each sampling, lids were left open for one hour to allow CO<sub>2</sub> equilibration with ambient air.

In the drying-rewetting experiment, soils were rewetted every 7 days by slowly adding Milli-Q water to reach 60% WHC. After water addition, jars were sealed, and headspace gas was sampled 6 hours later to capture Birch effect emissions. Soils were then dried to 5% WHC over the course of 2-3 days by removing the lids and incubating at ca. 25°C; respiration was not measured during this period.

### 323 2.3.2 Sampling schedule and CO<sub>2</sub> analysis

324 In the continuous wet experiment, headspace gas samples for CO<sub>2</sub> analysis were col-  
325 lected on days 1, 3, 5, 7, 11, 16, 27, 55, 82, 114, 151, and 225. After each sampling,  
326 jar lids were opened for one hour to equilibrate with ambient air.

327 In the drying–rewetting experiment, jars were sealed for 6 hours after water addi-  
328 tion, and headspace gas was sampled on days 1, 7, 21, 28, 35, 42, and 49 to evaluate the  
329 Birch effect. Control samples were collected on the same days for both experiments.

330 Evolved CO<sub>2</sub> concentrations were analyzed using a Shimadzu 2014 gas chromato-  
331 graph (Kyoto, Japan) with a thermal conductivity detector at UC Merced and an  
332 LI-830 infrared gas analyzer (IRGA) at Lawrence Livermore National Laboratory  
333 (LLNL).  
334

### 335 2.4 Statistical analyses

336 All statistical analyses were performed using CRAN-R 4.5.0 (R Core Team, 2025). Soil-  
337 respired CO<sub>2</sub> measurements from incubation experiments were averaged across two  
338 biological replicates per treatment. Control samples were represented by single mea-  
339 surements due to sample constraints. Accordingly, statistical comparisons involving  
340 controls were interpreted with caution.

341 The concentration of soil-respired CO<sub>2</sub> was expressed as the mass of C respired  
342 per unit mass of SOC, calculated as:  
343

$$344 \mu\text{g C} - \text{CO}_2 \text{ g soil C}^{-1} = \text{mmol air} * \frac{\mu\text{mmol CO}_2}{\text{mol air}} * \frac{10^{-3} \text{ mol air}}{\text{mmol air}} * \frac{12 \mu\text{g C}}{\mu\text{mol C}} * \frac{1}{\text{g TOC}} \quad (1)$$

345 For the continuously wet incubation, cumulative respiration was calculated by  
346 summing CO<sub>2</sub> fluxes over the 225-day experiment. Two-pool first-order decay models  
347 were fitted to cumulative respiration data according to:  
348

$$349 C_{\text{CO}_2}(t) = C_0 \left( 1 - (f_f e^{-k_f t} + f_s e^{-k_s t}) \right) \quad (2)$$

350 where  $C_{\text{CO}_2}(t)$  is the cumulative mass of C ( $\mu\text{g}$ ) respired by day  $t$ ,  $C_0$  denotes TOC,  
351  $f_f$  and  $f_s$  represent the fast- and slow-cycling fractions of SOC (with  $f_f + f_s = 1$ ),  
352 and  $k_f$  and  $k_s$  are the corresponding decay rate constants. Models were fitted using  
353 non-linear least-squares optimization with the `minpack.lm` package (Elzhov et al.,  
354 2023).

355 For the wet-dry cycling incubation, cumulative respiration was calculated by sum-  
356 ming CO<sub>2</sub> fluxes over wetting periods only, assuming negligible respiration during  
357 drying phases (Chaopricha, 2013). The effective incubation time ( $t$ ) was approximated  
358 as the cumulative duration of wetting events (2 days over a 49-day experiment).  
359 Two-pool decay models were initially fitted following the same approach as for the  
360 continuously wet incubation.

361 Preliminary model fits indicated that the fast-cycling pool contributed negligibly to  
362 respiration during wet-dry cycling (slow:fast pool ratio  $\sim 0.999:0.001$ ), consistent with  
363  
364  
365  
366  
367  
368

a functionally homogeneous system. Consequently, one-pool first-order decay models were also fitted for both incubation treatments:

$$C_{CO_2}(t) = C_0(1 - e^{-kt}) \quad (3)$$

where  $k$  represents the single-pool decomposition rate constant.

The effects of transect type, paleostatus, degree of burial or exposure, and their interactions on SOM decomposition parameters (decay rates and pool sizes) were evaluated using linear mixed-effects models, treating biological replicates as a random effect (controls excluded). These analyses were conducted using the `nlme` (Pinheiro et al., 2024) and `emmeans` (Lenth, 2024) packages. Significant differences among factor levels were assessed using pairwise Sidak-adjusted comparisons. For the wet-dry cycling experiment, similar models were applied to analyze day-1 CO<sub>2</sub> pulse responses.

Total CO<sub>2</sub> losses during wet-dry cycling (49 days) were compared to modeled CO<sub>2</sub> losses over an equivalent duration under continuous wetting using linear mixed-effects models with paleostatus, transect type, and degree of burial or exposure as fixed effects and replicate as a random effect. Marginal means and pairwise comparisons were used to contrast incubation treatments. For control samples, paleostatus and transect type were treated as fixed effects and degree of burial or exposure as a random effect. Despite limited replication, the large magnitude of difference between control and treatment fluxes (>45-fold) indicates that moisture addition, rather than incubation artifacts, drove observed respiration patterns.

Mean cumulative CO<sub>2</sub> losses between control and treatment groups were further compared using a Welch test following confirmation of unequal variances via a Bartlett test, implemented in the `stats` package (RStudio Team, 2019). Linear mixed-effects models were also used to evaluate the effects of transect type and paleostatus on cumulative CO<sub>2</sub> losses in control samples, with degree of burial or exposure treated as a random effect.

Multiple linear regression (MLR) was used to quantify the influence of soil physicochemical properties (soil pH, EC, TOC and TIC contents, SAR, texture, and exchangeable base cations) on modeled SOM decomposition parameters. For the continuously wet incubation, MLR models were applied to fast- and slow-pool decay rates and slow-pool fraction sizes derived from two-pool models. For the wet-dry cycling incubation, MLR analyses were conducted on decomposition rates derived from one-pool models. Model selection followed stepwise forward and backward procedures, prioritizing parsimony based on Akaike Information Criterion (AIC) values using the `MASS` package (Venables and Ripley, 2002). Model coefficients, intercepts, R<sup>2</sup>, and root mean squared error (RMSE) were calculated using the `stats` package. Pairwise Pearson correlation matrices were generated to visualize relationships among soil properties and SOM decomposition parameters using the `stats` and `ggplot2` packages (RStudio Team, 2019).

## 415 **3 Results**

416

### 417 **3.1 General soil properties**

418

419

420

421

422

423

424

425

426

427

428

429

430

431

432

433

434

### **3.2 Effects of continuous wetting on soil CO<sub>2</sub> efflux**

435

436

437

438

439

440

441

442

443

444

445

446

447

448

449

450

451

452

453

454

455

456

457

458

459

460

The physicochemical properties of soils used in the incubation experiment are shown in Table 5. The soils were relatively alkaline (pH ranging from 6.89 to 7.77), especially the Brady Soil (pH > 7.6). The clay, silt and sand content placed the soils in the texture class category of silt loam. Total organic carbon was higher in modern soils due to active biomass inputs, while inorganic carbon content was higher in the Brady Soil due to carbonate formation (Dolui et al., 2026b). The Brady soil of the burial transect was classified as saline (mean EC of 5.41 dS m<sup>-1</sup>) and the CEC of soils was moderately high, ranging from 15.17 - 23.31 cmol<sub>c</sub> kg<sup>-1</sup> and indicating the presence of higher activity clays. The turnover time of bulk soils as derived from radiocarbon-based models, was much greater in the Brady Soil (8327 - 15 654 years) compared to modern soils (576.4 - 1451 years), confirming the long-term stability of SOM in the paleosol (Dolui et al., 2026b). The mean CN ratio in both Brady and modern soils was relatively low (ca. 10), indicating a sufficient supply of N for plant growth and microbial activity.

In the continuous wet soil treatment group, modern soils evolved significantly higher CO<sub>2</sub> (mean of 30.6 mg CO<sub>2</sub>-C g C<sup>-1</sup>) compared to Brady Soil (mean of 15.9 ± 2.39 mg CO<sub>2</sub>-C g C<sup>-1</sup>) after 225 days of incubation (p < 0.01). Soils of the erosional transect type had greater cumulative C loss (mean of 29.3 mg CO<sub>2</sub>-C g C<sup>-1</sup>) compared to the burial transect (mean of 17.3 ± 2.39 mg CO<sub>2</sub>-C g C<sup>-1</sup>, p < 0.01). However, the difference between cumulative C losses of erosional vs burial transect types was not significant at the greatest degree of burial and lowest degree of erosion.

Modern soil in the erosional transect had significantly higher cumulative C losses (mean of 35.9 mg CO<sub>2</sub>-C g C<sup>-1</sup>) than modern soil of the burial transect (mean of 25.3 mg CO<sub>2</sub>-C g C<sup>-1</sup>, p < 0.05). Similarly, Brady Soil of the erosional transect had significantly higher cumulative C losses (mean of 22.6 mg CO<sub>2</sub>-C g C<sup>-1</sup>) compared to the burial transect (mean of 9.28 mg CO<sub>2</sub>-C g C<sup>-1</sup>, p < 0.05).

The Brady soil with an intermediate degree of erosion had higher cumulative CO<sub>2</sub> loss (mean of 33.2 mg CO<sub>2</sub>-C g C<sup>-1</sup>) compared to Brady Soil of the lowest and highest degrees of erosion, while the Brady soil with the greatest degree of burial had the lowest cumulative CO<sub>2</sub> loss (mean of 4.14 mg CO<sub>2</sub>-C g C<sup>-1</sup>, differences not significant). For Brady soil of the burial transect, the magnitude of cumulative CO<sub>2</sub> efflux among different degrees of burial was in the order of I > II > III, whereas in the erosional transect, cumulative CO<sub>2</sub> efflux among different degrees of erosion was II > III > I.

The cumulative CO<sub>2</sub> evolution of 60% WHC continuous wet experiments (mean of 23.3 mg CO<sub>2</sub>-C g C<sup>-1</sup>) was significantly greater than control soils maintained at 5% WHC (mean of 0.478 mg CO<sub>2</sub>-C g C<sup>-1</sup>, p < 0.001). Among the control soils, Brady

Soil of the burial transect had significantly greater C losses (mean of 0.561 mg CO<sub>2</sub>-C g C<sup>-1</sup>) compared to modern soils (mean of 0.253 ± 0.0683 mg CO<sub>2</sub>-C g C<sup>-1</sup>, p < 0.05), but C losses in modern and Brady Soil were more similar in the erosional transect (mean of 0.254 and 0.444 mg CO<sub>2</sub>-C g C<sup>-1</sup> for modern and Brady Soil respectively, n.s.).

Significance of differences in cumulative CO<sub>2</sub> losses among degree of burial/ exposure for control samples could not be tested due to lack of replication, but we report observed differences. Among the burial transect control soils, Brady soil with the lowest degree of burial produced the greatest cumulative CO<sub>2</sub> loss, while modern soil collected from the intermediate degree of burial soil produced the least cumulative CO<sub>2</sub> loss. Among the erosional transect control soils, the most CO<sub>2</sub> was evolved in the Brady soils with intermediate erosion, and the lowest CO<sub>2</sub> was evolved in the modern soil collected from the lowest degree of burial.

### 3.3 Effect of drying and rewetting on soil CO<sub>2</sub> efflux

Daily C lost from soils via respiration of CO<sub>2</sub> during the dry-rewetting incubation are shown in Fig. A1 and cumulative C losses are shown in Fig. 3. Soil respiration data from the dry-rewetting incubation are available online at DOI: doi: 10.17632/fjw646gpyf.1.

The largest respiration fluxes were produced on the first day, with significantly greater cumulative CO<sub>2</sub> loss from modern soils (mean of 0.920 mg CO<sub>2</sub>-C g C<sup>-1</sup>) compared to Brady Soil (mean of 0.729 ± 0.034 mg CO<sub>2</sub>-C g C<sup>-1</sup>, p < 0.01), but the reverse was observed at the greatest degree of burial. Respiration pulses declined over time for all soils. Control soils had a lower day<sup>-1</sup> pulse CO<sub>2</sub> (mean of 0.295 mg CO<sub>2</sub>-C g C<sup>-1</sup>) compared to the dry-rewetting treatment (mean of 0.824 mg CO<sub>2</sub>-C g C<sup>-1</sup>, p < 0.001), but there was no significant difference between the cumulative CO<sub>2</sub> loss from control (21.9 mg CO<sub>2</sub>-C g C<sup>-1</sup>) and treatments (17.5 mg CO<sub>2</sub>-C g C<sup>-1</sup>) by the final day of incubation.

After 49 days of incubation under wet-dry cycles, the Brady Soil from both the burial and the erosional transects emitted significantly more cumulative CO<sub>2</sub> (0.0183 g CO<sub>2</sub>-C g C<sup>-1</sup>) than Brady Soil incubated under continuously wet conditions (0.009 ± 0.0005 g CO<sub>2</sub>-C g C<sup>-1</sup>, p < 0.001). However, there was no significant difference between cumulative CO<sub>2</sub> loss in modern soils incubated under wet-dry cycles versus continuous wet conditions.

The order of magnitude of total CO<sub>2</sub> emission after 49 days followed the order erosional modern > erosional Brady > burial modern > burial Brady. Soils of the erosional transect (mean of 18.3 mg CO<sub>2</sub>-C g C<sup>-1</sup>) had significantly greater cumulative CO<sub>2</sub> loss compared to the burial transect (mean of 16.7 ± 0.643 mg CO<sub>2</sub>-C g C<sup>-1</sup>, p < 0.01). Modern soil had significantly greater cumulative CO<sub>2</sub> loss (mean of 16.7 mg CO<sub>2</sub>-C g C<sup>-1</sup>) than Brady Soil (mean of 18.3 ± 0.390 mg CO<sub>2</sub>-C g C<sup>-1</sup>, p < 0.001), but the difference was not significant at the intermediate degree of erosion. Modern soil with the highest degree of erosion emitted significantly more cumulative CO<sub>2</sub> (19.2 mg CO<sub>2</sub>-C g C<sup>-1</sup>) than modern soil with the greatest degree of burial (13.9 mg CO<sub>2</sub>-C g C<sup>-1</sup>, p < 0.05). However, the opposite was observed in Brady Soil, where that with the greatest degree of burial emitted more cumulative CO<sub>2</sub> (15.6 mg CO<sub>2</sub>-C g C<sup>-1</sup>) compared to the soil with the greatest degree of erosion (20.4 mg CO<sub>2</sub>-C g C<sup>-1</sup>,

507  $p < 0.05$ ). Among the control soils, although Brady Soil emitted more cumulative  
508  $\text{CO}_2$  than modern soil, there was no significant difference. This was likely due to large  
509 variation of the depth-pooled samples (in absence of control replicates), as a result of  
510 the much larger  $\text{CO}_2$  loss from Brady Soil of the erosional transect with the lowest  
511 degree of erosion compared to other samples.

512

### 513 **3.4 Decay rates and fraction sizes of soil organic matter pools**

514

515 The decomposition rate of the slow pool and size of the fast pool under continuous  
516 wetting is shown in Fig. 4 and the decomposition rate of SOM (single pool) under  
517 wet-dry cycles is shown in Fig. 5. Statistical figures of merit of linear mixed-effects  
518 models are available online at DOI : doi: [10.17632/fjw646gpyf.1](https://doi.org/10.17632/fjw646gpyf.1).

519

520 The slow-cycling SOM pool under continuous wetting decayed ca. 2000 times more  
521 slowly than the fast-cycling pool, with a significantly lower mean decay rate in the  
522 burial transect ( $8.68 \cdot 10^{-6} \text{ day}^{-1}$  i.e., 315 years turnover time, henceforth referred to  
523 as TOT) compared to the erosional transect ( $1.36 \cdot 10^{-5} \pm 6.82 \cdot 10^{-7} \text{ day}^{-1}$  i.e., 201  
524 years TOT,  $p < 0.01$ ). Thus, higher decay rates correspond to faster (shorter) turnover  
525 times throughout this section. The mean decay rate of the slow-cycling SOM pool of  
526 Brady Soil ( $6.86 \cdot 10^{-6} \text{ day}^{-1}$  i.e., 399 years TOT) was significantly lower than that  
527 of modern soil ( $1.54 \cdot 10^{-5} \text{ day}^{-1} \pm 6.82 \cdot 10^{-7}$ , i.e., 178 years TOT,  $p < 0.001$ ). The  
528 mean decay rate of the slow-cycling SOM pool of modern soil in the burial transect  
529 was significantly greater at the greatest degree of burial ( $1.53 \cdot 10^{-5} \text{ day}^{-1}$  i.e., 178  
530 years TOT), compared to the lowest degree of burial ( $9.97 \cdot 10^{-6} \text{ day}^{-1}$  i.e., 275 years  
TOT,  $p < 0.05$ ).

531

532 The mean decay rate of the fast-cycling SOM pool of the erosional transect ( $0.130$   
533  $\text{day}^{-1}$  i.e., 7.68 days TOT) under continuous wetting was significantly higher (i.e.,  
534 faster turnover) than that of the burial transect ( $0.126 \pm 0.001 \text{ day}^{-1}$  i.e., 7.96 days  
535 TOT,  $p < 0.05$ ). The mean decay rate of the fast-cycling SOM pool of Brady Soil in  
536 the erosional transect was significantly greater at the greatest degree of erosion ( $0.144$   
537  $\text{day}^{-1}$  i.e., 6.96 days TOT) compared to the lowest degree of erosion ( $0.121 \text{ day}^{-1}$  i.e.,  
8.25 days TOT,  $p < 0.01$ ).

538

539 The decay rate of SOM (one-pool model) under wet-dry cycles did not differ sig-  
540 nificantly among soils of different paleostatus or transect type. In the two-pool model,  
541 the decay rate of the slow-cycling SOM pool under wet-dry cycles was significantly  
542 higher in the erosional transect ( $0.007 \text{ day}^{-1}$  i.e., 129 days TOT) compared to the  
543 burial transect ( $0.009 \pm .0002 \text{ day}^{-1}$  i.e., 117 days TOT,  $p < 0.05$ ), indicating faster  
544 SOM turnover where decay rates were higher. The decay rate of the fast-cycling SOM  
545 pool in the burial transect was significantly higher in modern soil ( $8.11 \pm 1.94 \text{ day}^{-1}$   
i.e., 0.123 days TOT) compared to Brady soil ( $0.558 \text{ day}^{-1}$  i.e., 1.79 days TOT).

546

547 The slow-cycling pools of both modern and Brady Soil under continuous wetting  
548 contained a much greater proportion of total SOC ( $> 96\%$ ) than the fast-cycling  
549 pool. The fraction size of the fast-cycling pool relative to the slow-cycling pool under  
550 continuous wetting was significantly greater in the erosional transect (0.014) compared  
551 to the burial transect ( $0.012 \pm 0.0003$ ,  $p < 0.01$ ) and significantly greater in modern  
552 soils (0.0173) compared to Brady Soil ( $0.009 \pm 0.0003$ ,  $p < 0.001$ ). The fraction size  
of the fast and slow pools tended to 0 and 1.0 respectively in all soils under wet-dry

cycling, nullifying the statistical comparison results among soils of different paleostatus and transect types. 553  
554

### 3.5 Decay rates and fraction sizes of soil organic matter pools in continuous wet versus wet-dry experiment 555 556 557

A summary of SOM decomposition model parameters (one-pool and two-pool) of the continuously wet and wet-dry cycling experiments is shown in Table 2. Statistical figures of merit of linear mixed-effects models are available online at DOI : doi: 558  
559  
560  
561  
562

With the one-pool models, the continuously wet soils had a significantly higher decay rate ( $0.00865 \text{ day}^{-1}$  i.e., 116 days TOT) compared to the wet-dry cycles ( $0.00714 \text{ day}^{-1}$  i.e., 140 days TOT,  $p < 0.01$ ), indicating faster turnover under continuous wetting. In the burial transect, the one-pool decay constant of the continuous wet experiment was significantly higher ( $0.0103 \text{ day}^{-1}$  i.e., 97.4 days TOT) than that of the wet-dry cycling experiment ( $0.00690 \text{ day}^{-1}$  i.e., 145 days TOT,  $p < 0.001$ ). However, there was no significant difference between the decay constant of the continuous wet and wet-dry experiments in erosional transects. These trends were observed in both Brady and modern soils. 563  
564  
565  
566  
567  
568  
569  
570  
571

Among the control soils with one-pool models, the continuous wet experiment had a significantly higher decay rate ( $0.0376 \text{ day}^{-1}$  i.e., 26.6 days TOT) compared to the wet-dry cycling experiment ( $0.00146 \text{ day}^{-1}$  i.e., 179 days TOT,  $p < 0.001$ ), again meaning faster decomposition under continuous wetting. This was true in both burial (continuous wet  $k = 0.0374 \text{ day}^{-1}$  i.e., 26.7 days TOT and wet-dry  $k = 0.00372$  i.e., 268 days TOT) and erosional ( $k = 0.0377 \text{ day}^{-1}$  i.e., 26.5 days TOT and wet-dry  $k = 0.00746 \text{ day}^{-1}$  i.e., 134 days TOT) transects, as well as Brady (continuous wet  $k = 0.0376 \text{ day}^{-1}$  i.e., 26.6 days TOT and wet-dry  $k = 0.00871 \text{ day}^{-1}$  i.e., 115 days TOT) and modern (continuous wet  $k = 0.0375 \text{ day}^{-1}$  i.e., 26.7 days TOT and wet-dry  $k = 0.00248 \text{ day}^{-1}$  i.e., 404 days TOT) soils. 572  
573  
574  
575  
576  
577  
578  
579  
580  
581

With the two-pool models, the decay rate of the slow-cycling SOM pool in the continuously wet experiment was significantly lower ( $1.11 \cdot 10^{-5} \text{ day}^{-1}$  i.e., 246 years TOT) than that of the wet-dry cycling experiment ( $0.00812 \text{ day}^{-1}$  i.e., 123 days TOT,  $p < 0.001$ ), reflecting faster turnover in the wet-dry treatments. This was true in both Brady (continuously wet  $k = 6.86 \cdot 10^{-6} \text{ day}^{-1}$  i.e., 399 years TOT, wet-dry  $k = 0.0083 \text{ day}^{-1}$  i.e., 120 days TOT) and modern (continuously wet  $k = 1.54 \cdot 10^{-5} \text{ day}^{-1}$  i.e., 178 years TOT, wet-dry  $k = 0.00793 \text{ day}^{-1}$  i.e., 126 days TOT) soils, as well as both burial (continuously wet  $k = 8.68 \cdot 10^{-6} \text{ day}^{-1}$  i.e., 316 years TOT, wet-dry  $k = 0.00773 \text{ day}^{-1}$  i.e., 129 days TOT) and erosional (continuously wet  $k = 1.36 \cdot 10^{-5} \text{ day}^{-1}$  i.e., 202 years TOT, wet-dry  $k = 0.0085 \text{ day}^{-1}$  i.e., 118 days TOT) transects, and at all degrees of burial and erosional exposure. 582  
583  
584  
585  
586  
587  
588  
589  
590  
591  
592

The decay rate of the fast-cycling SOM pool in modern soil was significantly higher in the wet-dry cycling experiment ( $8.11 \text{ day}^{-1}$  i.e., 0.123 days TOT) compared to the continuously wet experiment ( $0.127 \text{ day}^{-1}$  i.e., 7.89 days TOT,  $p < 0.001$ ), indicating a much faster turnover response to rewetting. The decay rate of the fast-cycling pool in the erosional transect was also significantly higher in the wet-dry cycling experiment ( $5.148 \text{ day}^{-1}$  i.e., 0.194 days TOT) compared to the continuously wet 593  
594  
595  
596  
597  
598  
599

599 experiment ( $0.130 \text{ day}^{-1}$  i.e., 7.68 days TOT). Separating these effects by degree of  
600 erosional exposure revealed that the significance of the difference between the fast pool  
601 decay rate in modern soils was more evident at the intermediate and lowest degree  
602 of erosion. The decay rate of the fast-cycling SOM pool did not differ significantly  
603 between continuously wet and wet-dry cycling experiments in Brady soils or in the  
604 burial transect.

605 Among the control soils with two-pool models, the continuous wet experiment had  
606 significantly lower slow pool decay rate ( $1 \cdot 10^{-8} \text{ day}^{-1}$  i.e., 274 000 years TOT)  
607 compared to the wet-dry cycling experiment ( $k = 0.005 \text{ day}^{-1}$  i.e., 200 days TOT,  $p$   
608  $< 0.01$ ), again corresponding to much faster turnover in the wet-dry treatments. This  
609 was true in both the burial and erosional transects, modern and Brady Soil and at all  
610 degrees of erosion and burial.

611 In contrast to the main soil dataset described above, the decay rate of the fast-  
612 cycling SOM pool of control Brady Soil was significantly higher in the wet-dry cycling  
613 experiment ( $0.0556 \text{ day}^{-1}$  i.e., 18.0 days TOT) compared to the continuously wet  
614 experiment ( $10.3 \text{ day}^{-1}$  i.e., 0.0971 days TOT). This was true in both burial and  
615 erosional transects. In modern control soils, however, there was no significant difference  
616 between decay rates of fast-cycling SOM in continuously wet versus wet-dry cycling  
617 experiments.

618 The fraction size of the slow-cycling SOM pool in the wet-dry cycling experiment  
619 was significantly larger (0.999) than that of the continuously wet experiment (0.987,  $p$   
620  $< 0.001$ ) - this was true for both Brady and modern soils, across erosional and burial  
621 transects and at all degrees of erosion and burial. It follows that the fraction size of  
622 the fast-cycling SOM pool in wet-dry cycling experiments was significantly smaller  
623 (0.001) than that of the continuously wet experiment (0.0131,  $p < 0.001$ ) for soils of  
624 all transect types, paleostatus groups and degrees of erosion and burial. There was  
625 no significant difference between fraction sizes of the slow-cycling SOM pool among  
626 the controls of the wet-dry cycling and continuously wet experiment; the fast-cycling  
627 pool was also similar among control soils of the two experiments.

628

### 629 **3.6 Relationships between soil properties and carbon dynamics**

630

631 The true versus predicted values MLR models for prediction of decomposition rates of  
632 the fast- and slow-cycling pools as well as the fraction size of the slow pool are shown  
633 in the Appendix, Fig. A2. A matrix showing the correlation between these variables is  
634 given in Fig. 6. The intercept, coefficients of explanatory variables, RMSE and  $R^2$  of  
635 the best-performing MLR models, are summarized in Table 3 and the full equations  
636 are in the Appendix (Multiple linear regression equations).

637 The MLR models for prediction of decay rates of SOM under continuous wetting  
638 had better model fit ( $R^2 > 0.80$ ) compared to those for predictions of SOM pool  
639 fraction size ( $R^2 = 0.44$ ). From the MLR equations, we deduce that soil properties with  
640 the greatest coefficients had the most important effects on the SOM decay rate and  
641 fraction size model parameters. While SAR increased the rate of decay and decreased  
642 the size of the of the slow pool, an opposite trend is observed in the fast pool.

643 TOC and pH also increased the decay rate of the fast-cycling SOM pool under  
644 continuous wetting, while the slow pool decay rate decreased with increasing TIC.

TOC and TIC increased the fraction size of the slow pool at the expense of fraction size of the fast pool. When considering effects of these factors individually, SAR, TOC, TIC and pH did not have significant correlation with SOM decomposition parameters (Fig. 6). However, exchangeable Mg and K content were significantly correlated with the decay rate of the fast (negative correlation) and slow (positive correlation) pools (Fig. 6).

The true versus predicted values MLR models for prediction of the decomposition rate of SOM (one-pool system) under wet-dry cycles are shown in the Appendix, Fig A3. A matrix showing the correlation between these variables is given in Appendix, Fig. A4.

The intercept, coefficients of explanatory variables, RMSE and  $R^2$  of the best-performing MLR model for prediction of the decay rate, are given summarized in Table 3 and the full equation is in the Appendix (Multiple linear regression equations).

SAR decreased the decay rate of SOM under wet-dry cycles. Clay and TOC content increased the decay rate of SOM. Exchangeable Ca, Mg content decreased the decay rates of both pools. Considering these parameters individually (correlation coefficients) revealed a weak correlation with k. Therefore MLR, where k is modeled as a function of all predictors together, demonstrates that the combination of these variables explained most variance, while no single predictor explained much variance on its own.

## 4 Discussion

### 4.1 Stabilization of soil organic matter by burial

While our study characterizes decomposition dynamics using respirometry and radiocarbon-based modeling, we did not directly measure the molecular mechanisms responsible for differential SOC stability. Specifically, we did not quantify the chemical composition of mineral-associated organic matter, the nature of organo-mineral bonds, or microbial community composition. As a result, the mechanistic interpretations presented here are necessarily indirect.

The interpretations proposed in this study build on prior molecular and fractionation-based analyses conducted on the same soils and geomorphic transects (Marin-Spiotta et al., 2014; Dolui et al., 2026b). That work documented enhanced mineral association and cation-mediated stabilization in buried profiles. Rather than repeating those analyses, the present study extends this framework by quantifying how these stabilization contexts translate into differences in SOC turnover rates and pool structure under contrasting moisture regimes.

Brady Soil subjected to continuous wetting exhibited lower cumulative  $\text{CO}_2$  evolution than modern soils across both erosional and burial transects (Fig. 2; Appendix Fig. 3). This pattern indicates reduced microbial mineralization in buried paleosols relative to surface soils under sustained moisture availability.

Multiple mechanisms may contribute to this enhanced stability, although their relative importance cannot be resolved with the current dataset. Previous work at this site reported elevated exchangeable  $\text{Ca}^{2+}$  concentrations in Brady soils and linked Ca-mediated flocculation to increased aggregate stability (Dolui et al., 2026a). Our results are consistent with this interpretation. Specifically, Ca concentration was a

691 positive predictor of slow-pool size in the MLR model. However, we did not directly  
692 measure aggregation or flocculation processes. As a result, the pathway linking Ca  
693 availability to reduced decomposition remains uncertain. Reduced decay could arise  
694 from physical protection within aggregates, reduced microbial access to substrates, or  
695 changes in solute diffusivity (Six et al., 2002). Within the scope of this study, Ca<sup>2+</sup>  
696 therefore emerges as a statistically robust predictor of SOC pool structure, rather than  
697 a resolved mechanistic driver.

698 The potential contribution of pyrogenic carbon to SOC persistence in Brady soils  
699 is supported by prior molecular analyses from this site. These analyses identified con-  
700 densed aromatic compounds consistent with fire-derived inputs (Marin-Spiotta et al.,  
701 2014). Pyrogenic carbon was not quantified in the present study, and its direct influ-  
702 ence on decomposition rates cannot be evaluated here. Nonetheless, its documented  
703 persistence provides important context for interpreting the slow-cycling SOC pool  
704 observed in Brady soils. Our results are therefore compatible with a stabilization legacy  
705 established during Brady Soil formation, rather than evidence of an active pyrogenic  
706 control on contemporary decomposition.

707 Modern soils exhibited a slightly larger relative size of the fast-cycling SOM pool  
708 than Brady soils, which likely reflects recent organic inputs. Direct comparison of  
709 decay parameters further highlights differences in SOM persistence between soil types  
710 (Fig. 4). The slow-cycling pool in Brady soils from the most erosional transect had  
711 significantly lower decay rates under continuous wetting than the corresponding pool in  
712 modern soils. This provides clear evidence of greater SOM persistence in the paleosol.

713 Across all treatments, the slow pool decayed approximately 2000 times more slowly  
714 than the fast pool (Appendix, Fig. A2). The slow-cycling pool of the Brady Soil exhib-  
715 ited a turnover time (TOTs) of approximately 399 years, whereas the slow-cycling  
716 pool of modern soil exhibited a TOT of approximately 178 years. The MLR mod-  
717 els further showed a negative relationship between slow-pool decay rate ( $k_{\text{slow}}$ ) and  
718 both total inorganic carbon (TIC) and exchangeable Mg<sup>2+</sup> (Equation A1). Although  
719 CaCO<sub>3</sub> cementation was not pronounced, positive correlations between TOC, TIC,  
720 and Ca in Brady soils from erosional transects (Dolui et al., 2026a) suggest that  
721 carbonate-associated phases may contribute to stabilization where shallow wetting  
722 promotes near-surface carbonate precipitation.

723 The association between finer texture and reduced SOC decomposition observed in  
724 this study aligns with established theory linking clay-rich soils to enhanced mineral-  
725 associated organic matter formation (Six et al., 2002). Clay content was a significant  
726 predictor of slow-pool dynamics in the MLR models, indicating that particle size exerts  
727 a first-order control on SOC accessibility. However, because mineral surface chemistry  
728 and sorption energetics were not resolved, texture is interpreted here as a proxy for  
729 stabilization potential rather than as a direct mechanistic control, given the complexity  
730 of detangling texture and mineralogical controls (Rasmussen et al., 2018).

731 The slow-cycling SOM pool dominated total soil C, accounting for more than  
732 96% of SOC (Fig. 4b). The size of this pool increased with increasing TOC and TIC  
733 (Equation A1) and was accompanied by a corresponding decline in the fast-cycling  
734 pool. The fast pool consistently represented a larger fraction of total SOC in modern  
735 soils than in Brady soils, and in erosional transects than in burial transects. Together,  
736

these patterns indicate stronger stabilization in buried paleosols and underscore the central role of the slow-cycling pool in long-term SOC persistence.

Apparent relationships between sodium adsorption ratio (SAR), exchangeable cations, decay rates, and pool sizes in the MLR models (Equations A1, A2, A3, and A4; Fig. 6) should be interpreted cautiously. These correlations may reflect shared depth-dependent trends rather than direct mechanistic links. Both TOC and microbial biomass typically decline with depth (Fierer and Schimel, 2003; Xiang et al., 2008), which contributes to reduced respiration in deeper Brady soils. At the same time, Na tends to accumulate at depth through leaching (Dolui et al., 2026a), with accumulation depth depending on precipitation and soil water status.

## 4.2 Destabilization of SOM by erosion and moisture variability

Greater cumulative C loss from shallower soils, combined with a smaller fast-cycling SOM pool and a significantly higher slow-pool decay rate in erosional Brady soils compared to burial Brady soils (Fig. 4a), highlights the destabilizing effect of surface exposure. This pattern indicates that erosion weakens burial-associated protection.

CO<sub>2</sub> pulses during the initial phase of wet–dry cycling were larger in erosional transects than in burial transects (Fig. A1). These pulses suggest enhanced mineralization in Brady soils closer to the surface. One likely explanation is priming by root exudates and fresh organic inputs, amplified by bioturbation (Pausch et al., 2016; McMurtry et al., 2024). This interpretation is supported by higher fraction modern values in erosional Brady soils relative to burial Brady soils, as well as by convergence of slow-pool fraction modern values toward those of modern soils (Dolui et al., 2026b).

Enhanced decomposition in shallower Brady soils likely reflects both legacy exposure and contemporary environmental conditions. Shallower positions experience more frequent wetting and greater oxygen diffusion, which can prime microbial communities for rapid response following rewetting. Separating long-term exposure effects from ongoing environmental controls would require experimental manipulation of burial depth, which represents an important avenue for future research.

In the wet–dry experiment, erosion effects were further expressed in decay dynamics. Slow pools decayed faster in erosional transects than in burial transects, whereas fast pools decomposed more rapidly in modern soils than in Brady soils. The fraction of the slow pool was smaller under continuous wetting than under wet–dry cycling, indicating greater allocation to slow-cycling carbon under variable moisture. However, the slow pool also exhibited substantially higher decay rates under wet–dry cycling. This suggests that apparent stabilization under variable moisture is transient and may be offset over time by depletion of passive C reserves.

The accelerated decay of slow-pool SOC under drying–rewetting cycles demonstrates that burial-associated protection is not absolute, even for millennially persistent carbon. Potential mechanisms include aggregate disruption, increased solute transport, or shifts in microbial accessibility. While the present study cannot resolve these pathways, it clearly documents the outcome: enhanced decomposition of previously slow-cycling SOC under moisture variability.

783 Moisture variability also amplified turnover of the fast-cycling pool. Decay rates  
784 of the fast pool increased under wet–dry cycling, particularly in modern soils and ero-  
785 sional transects. This pattern supports the interpretation that fresh organic inputs and  
786 surface exposure accelerate labile C turnover under fluctuating moisture. The MLR  
787 model reinforces this interpretation by revealing a positive relationship between TOC  
788 and fast-pool decay rate (Equation A4). In contrast, the absence of strong moisture  
789 effects in Brady soils suggests that burial dampens moisture-driven variability in labile  
790 C decomposition.

791 McDowell et al. (2022) simulated soil hydrology for the Brady Soil, overlying loess,  
792 and modern soil using measured hydraulic properties and regional weather data from  
793 2009–2019. Modeled water contents remained low and relatively constant below 1.5 m  
794 depth from the surface, including within the Brady Soil, with only rare deep wetting  
795 events following major rainfall. Paleoclimate reconstructions indicate that the depth  
796 of frequent wetting would have been even shallower during drier-than-modern periods  
797 over the past 10,000 years (Miao et al., 2007). Together, these results suggest that  
798 prolonged dry conditions played a major role in OC sequestration where the Brady  
799 Soil is deeply buried, whereas erosion and increased moisture variability could promote  
800 renewed C loss.

801 Geomorphic position integrates multiple stabilization controls by regulating burial  
802 depth, moisture exposure, oxygen availability, and the persistence of mineral–organic  
803 associations. In this sense, geomorphic context operates as a higher-order constraint  
804 that modulates how chemical and physical stabilization mechanisms are expressed  
805 through time. This aligns with conceptual frameworks suggesting that spatial patterns  
806 of soil organic carbon (SOC) are fundamentally shaped by the interplay between bio-  
807 logical cycling and geomorphic processes like erosion and deposition (Yoo et al., 2006).  
808 Furthermore, topography acts as a primary control on SOC distribution by mediating  
809 local microclimate and the lateral transport of soil material across mantled landscapes  
810 (Patton et al., 2019). These findings challenge the common assumption in soil carbon  
811 modeling that geomorphic context can be neglected when parameterizing decompo-  
812 sition rates. Recent evidence underscores that geomorphic settings not only dictate  
813 the abundance of SOC but also the persistence of specific carbon pools, particularly  
814 in erosional landscapes where geomorphic history defines the vulnerability of buried  
815 carbon (Hunter et al., 2024). Our results show that erosional exposure accelerates slow-  
816 pool decay under continuous wetting, and that wet–dry cycling destabilizes slow-pool  
817 carbon regardless of landscape position. For Earth system models that treat subsoil  
818 carbon as a passive reservoir, these dynamics represent a substantial and underappre-  
819 ciated vulnerability. Accurately predicting SOC responses to changing precipitation  
820 regimes therefore requires explicit consideration of burial depth and exposure history,  
821 which are rarely incorporated into current modeling frameworks.

822

## 823 5 Conclusion

824

825 When interpreted alongside prior molecular- and fractionation-based analyses from  
826 this site (Marin-Spiotta et al., 2014; Dolui et al., 2026a,b), our results suggest that

827

828

long-term SOC persistence in Brady soils arises from the convergence of mineral association, cation-mediated stabilization, and limited environmental exposure. The present study extends this framework by demonstrating that these stabilization contexts remain vulnerable to hydrologic perturbation and geomorphic re-exposure. Although this study does not resolve molecular-scale mechanisms directly, it demonstrates that decomposition parameters derived from incubation and radiocarbon modeling are highly sensitive to landscape history – an effect that must be accounted for even when detailed chemical data are unavailable.

Our study demonstrates that SOC decomposition is strongly shaped by soil moisture regime and landscape position, with modern and Brady soils responding differently to continuous wetting versus drying–rewetting cycles. Water availability exerted disproportionate effects in erosional settings where surface exposure enhanced substrate diffusivity, highlighting the destabilizing role of re-exposure and moisture fluctuations.

Drying–rewetting cycles led to greater C losses from Brady soils than continuous wetting, despite modeling results indicating dominance of the slow pool and depletion of labile C. This treatment also accelerated fast pool decay in modern soils and erosional transects, while burial dampened such variability in Brady soils. Fraction sizes shifted accordingly: wet–dry cycles increased the proportion of the slow pool and reduced the fast pool fraction, suggesting redistribution of SOC toward more stabilized forms under fluctuating moisture.

Depth further constrained SOM persistence, with slow pool decay constants declining with increasing degree of burial in Brady soils from burial transects. Faster turnover in shallow layers reflects greater microbial accessibility and responsiveness to surface-driven processes, underscoring the importance of geomorphic context - transect type, degree of burial, and soil structure - over intrinsic SOM chemistry.

Comparisons across models showed that continuous wetting accelerated overall decay, particularly in burial transects, while wet–dry cycles disproportionately destabilized the slow pool that dominates SOC. This dual effect - rapid labile C turnover under moisture fluctuations coupled with erosion of long-lived SOM persistence - points to heightened vulnerability of buried carbon under future precipitation variability.

Overall, the fate of ancient soil carbon under climate change will depend on both its burial history and prevailing moisture regime. Integrating these contrasting controls on fast- and slow-cycling pools into Earth system models is essential for improving predictions of soil carbon vulnerability and climate feedback.

**Funding.** This work was supported by the National Science Foundation (EAR awards 1623814, 1623810, and 1623812), the University of California, Merced, and the Ted and Jan Falasco Endowment.

**Competing interests.** The authors have no relevant financial or non-financial interests to disclose.

**Data availability.** Full dataset for soil incubation and statistical analyses are available at DOI: doi: 10.17632/fjw646gpyf.1.

875 **Author contributions.** All authors contributed to the study conception and  
876 design. Material preparation, data collection, and analysis were performed by Man-  
877 isha Dolui, Teneille Nel, Abbygail R. McMurtry, Stephanie Chacon, Laura M. Phillips,  
878 Teamrat Ghezzehei, Joseph A. Mason, Erika Marin-Spiotta, Marie-Anne de Graaff  
879 and Asmeret Asefaw Berhe. The first draft of the manuscript was written by Manisha  
880 Dolui and Teneille Nel. All authors commented on previous versions of the manuscript  
881 and approved the final manuscript.

882 **Acknowledgments.** We acknowledge financial support for this work from the  
883 National Science Foundation (EAR awards 1623814, 1623810, and 1623812) and the  
884 Ted and Jan Falasco Endowment, fellowships and grants awarded by the Graduate  
885 Division at the University of California, Merced (UCM), and the UCM Environmen-  
886 tal Systems Graduate Group. We are grateful to Dr. Sora Kim and Dr. Robin Trayler  
887 for their support at the UCM Stable Isotope Lab. We also thank R. and D. Whiting  
888 for providing access to the Wauneta, Nebraska, field sites. ChatGPT was used for lan-  
889 guage editing and sentence refinement and the authors take full responsibility for the  
890 output.  
891

892  
893  
894  
895  
896  
897  
898  
899  
900  
901  
902  
903  
904  
905  
906  
907  
908  
909  
910  
911  
912  
913  
914  
915  
916  
917  
918  
919  
920

Tables and figures.

921  
922  
923  
924  
925  
926  
927  
928  
929  
930  
931  
932  
933  
934  
935  
936  
937  
938  
939  
940  
941  
942  
943  
944  
945  
946  
947  
948  
949  
950  
951  
952  
953  
954  
955  
956  
957  
958  
959  
960  
961  
962  
963  
964  
965  
966

967  
 968  
 969  
 970  
 971  
 972  
 973  
 974  
 975  
 976  
 977  
 978  
 979  
 980  
 981  
 982  
 983  
 984  
 985  
 986  
 987  
 988  
 989  
 990  
 991  
 992  
 993  
 994  
 995  
 996  
 997  
 998  
 999  
 1000  
 1001  
 1002  
 1003  
 1004  
 1005  
 1006  
 1007  
 1008  
 1009  
 1010  
 1011  
 1012

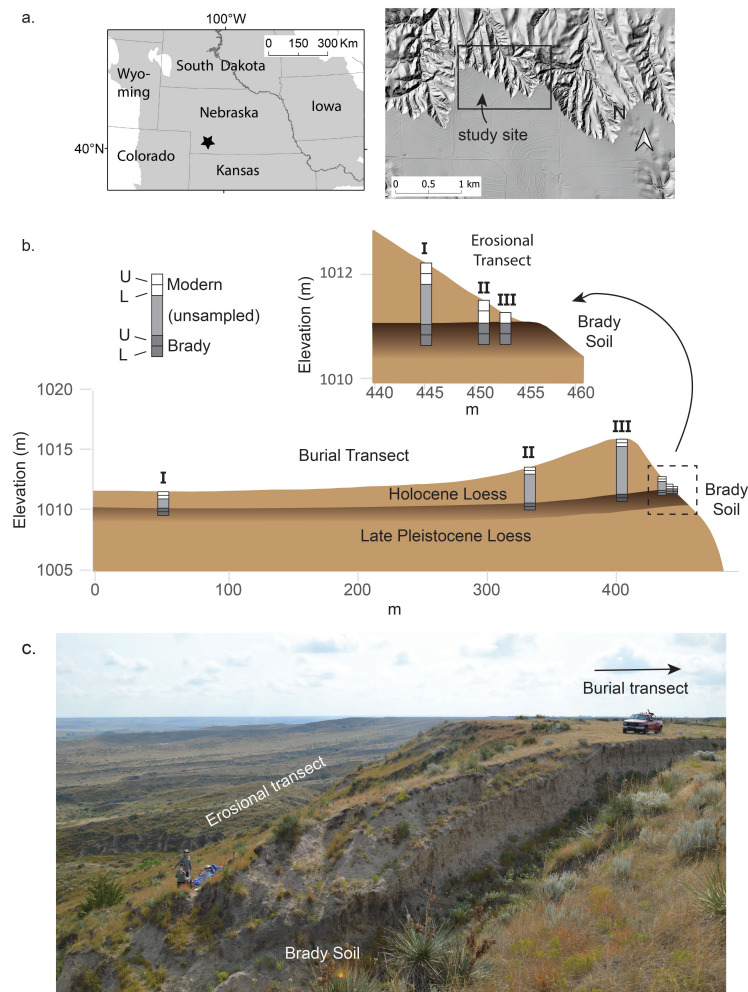


**Fig. 1** Study site location, stratigraphy, and sampling scheme. a. Location of the study site within the Great Plains ecoregion (grayshade) and shaded relief map illustrating topographic setting of study site. b. Vertical cross-sections illustrating the sampling scheme relative to modern land surface topography, the Brady Soil, and loess above and below it at study site. Weakly developed horizons of modern soil and paleosols within the Holocene loess (Miao et al., 2007) not shown. Details based on one pair of burial and erosional transects but representative of all three. c. Photo illustrating topography and native grassland vegetation at one pair of transects. Truck is near deepest profile (III) on burial transect; other burial transect points are not visible. Brady Soil is exposed in an old roadcut in foreground; erosional transect is located on intact slope beyond roadcut. Figure adapted from [Dolui et al. \(2026b\)](#)

1013  
 1014  
 1015  
 1016  
 1017  
 1018  
 1019  
 1020  
 1021  
 1022  
 1023  
 1024  
 1025  
 1026  
 1027  
 1028  
 1029  
 1030  
 1031  
 1032  
 1033  
 1034  
 1035  
 1036  
 1037  
 1038  
 1039  
 1040  
 1041  
 1042  
 1043  
 1044  
 1045  
 1046  
 1047  
 1048  
 1049  
 1050  
 1051  
 1052  
 1053  
 1054  
 1055  
 1056  
 1057  
 1058

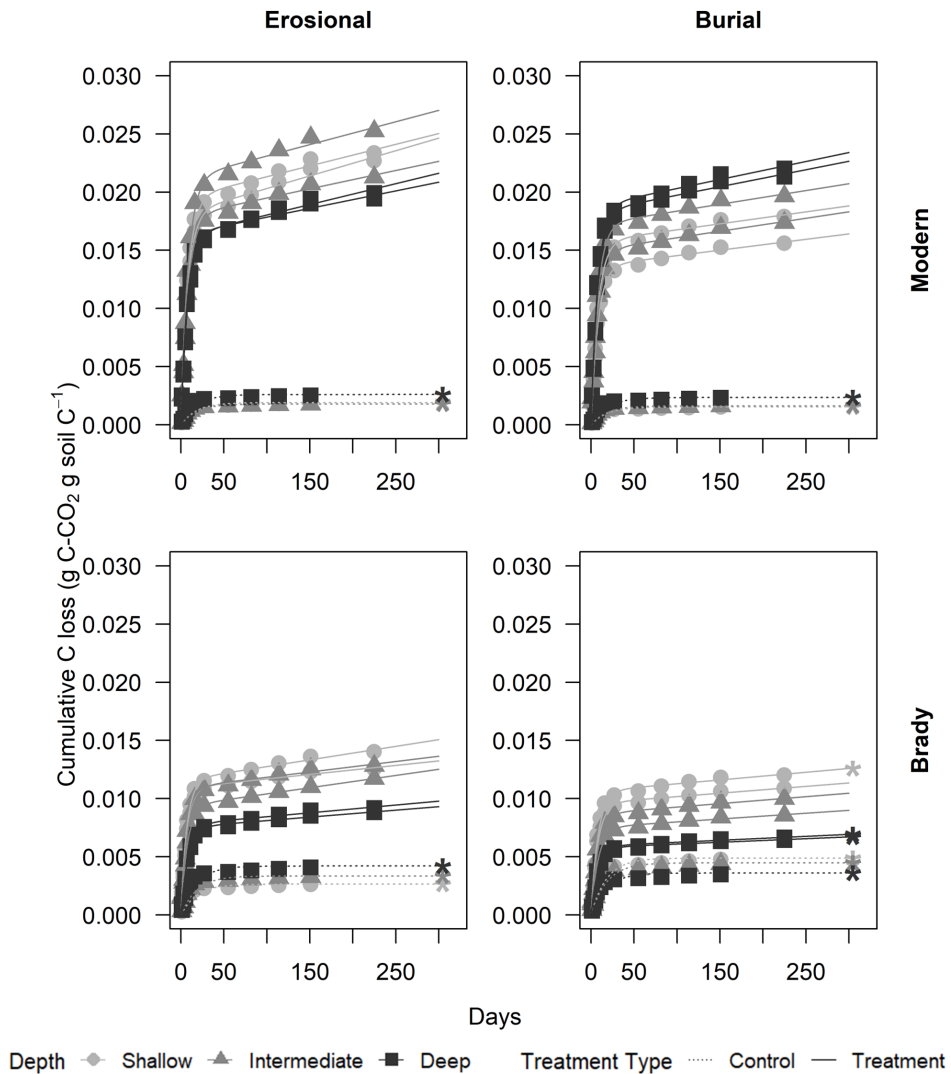


**Fig. 2** Cumulative respiratory CO<sub>2</sub> from modern and Brady Soil sampled from three depths representing varying degrees of burial/erosional exposure (two technical replicates each). In burial transects, Shallow → Intermediate → Deep corresponds to burial degrees I → II → III. In erosional transects, this relationship is reversed, with Shallow → Intermediate → Deep corresponding to exposure degrees III → II → I. Soils were maintained at a constant moisture content of 60% water holding capacity (WHC). Lines depict a two-pool first-order decay model, fitted using a non-linear least-squares function. The dotted line represents the control (5% WHC).

1059  
 1060  
 1061  
 1062  
 1063  
 1064  
 1065  
 1066  
 1067  
 1068  
 1069  
 1070  
 1071  
 1072  
 1073  
 1074  
 1075  
 1076  
 1077  
 1078  
 1079  
 1080  
 1081  
 1082  
 1083  
 1084  
 1085  
 1086  
 1087  
 1088  
 1089  
 1090  
 1091  
 1092  
 1093  
 1094  
 1095  
 1096  
 1097  
 1098  
 1099  
 1100  
 1101  
 1102  
 1103  
 1104

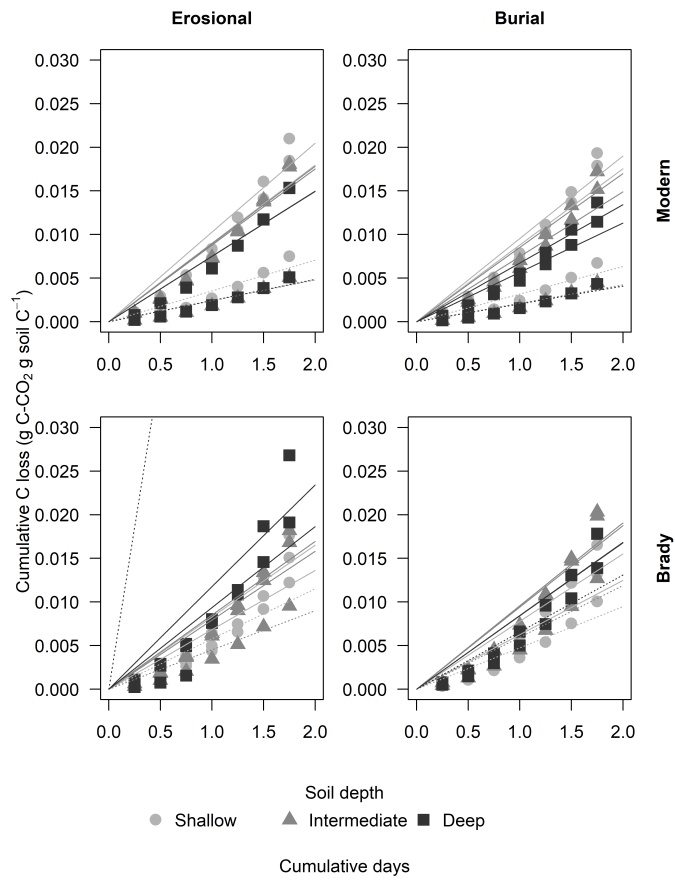


**Fig. 3** Cumulative respiratory CO<sub>2</sub> flux from modern and Brady Soil sampled from three depths representing varying degrees of burial/erosional exposure (two technical replicates each). In burial transects, Shallow → Intermediate → Deep corresponds to burial degrees I → II → III. In erosional transects, this relationship is reversed, with Shallow → Intermediate → Deep corresponding to exposure degrees III → II → I. Soils were wetted to a moisture content of 60% water holding capacity (WHC) and allowed to dry to 5% WHC. Lines depict a one-pool first-order decay model, fitted using a non-linear least-squares function. The dotted line represents the control (constant 5% WHC); one control Brady soil sample of the erosional transect had an outlier point not shown due to scale. Asterisks (\*) indicate control samples maintained at 5% WHC

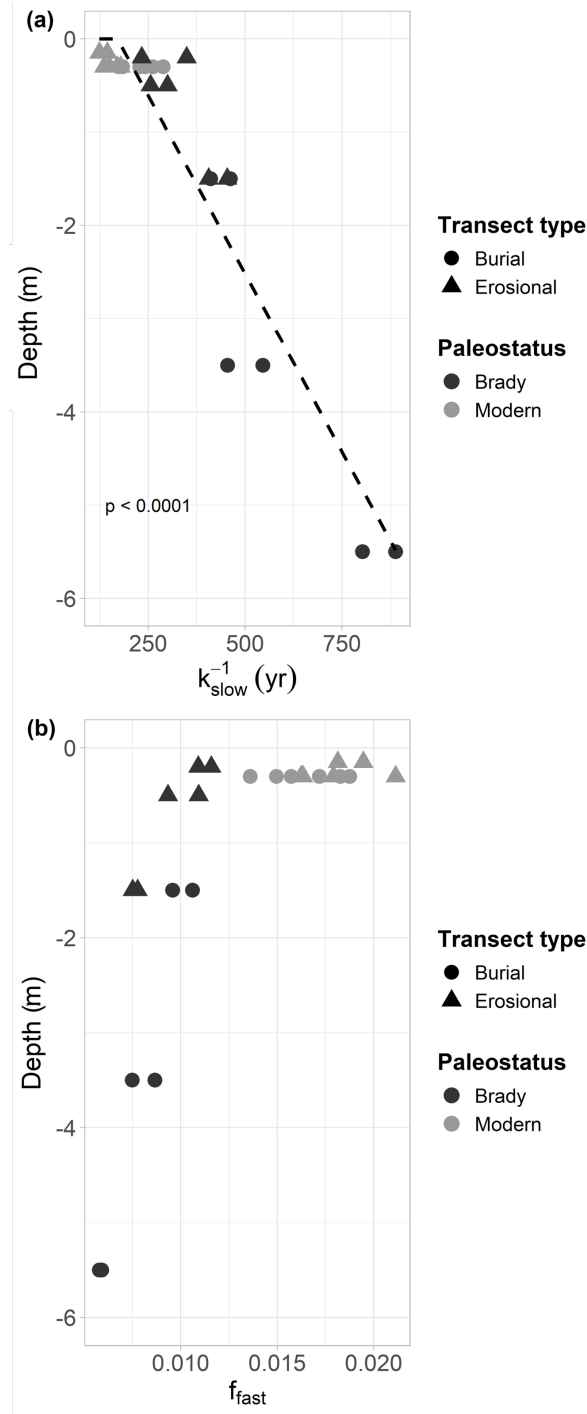


**Fig. 4** Decay constant of the slow cycling pool of modern and Brady soils at different depths (from the soil surface), incubated under continuously wet conditions. Samples collected from burial and erosional transect types. Dotted line indicates exponential decay. Figure b indicates the size of the fast-cycling pool at different depths (from the soil surface) of the modern and Brady soils in burial and erosional transect types.

1105  
 1106  
 1107  
 1108  
 1109  
 1110  
 1111  
 1112  
 1113  
 1114  
 1115  
 1116  
 1117  
 1118  
 1119  
 1120  
 1121  
 1122  
 1123  
 1124  
 1125  
 1126  
 1127  
 1128  
 1129  
 1130  
 1131  
 1132  
 1133  
 1134  
 1135  
 1136  
 1137  
 1138  
 1139  
 1140  
 1141  
 1142  
 1143  
 1144  
 1145  
 1146  
 1147  
 1148  
 1149  
 1150

1151  
 1152  
 1153  
 1154  
 1155  
 1156  
 1157  
 1158  
 1159  
 1160  
 1161  
 1162  
 1163  
 1164  
 1165  
 1166  
 1167  
 1168  
 1169  
 1170  
 1171  
 1172  
 1173  
 1174  
 1175  
 1176  
 1177  
 1178  
 1179  
 1180  
 1181  
 1182  
 1183  
 1184  
 1185  
 1186  
 1187  
 1188  
 1189  
 1190  
 1191  
 1192  
 1193  
 1194  
 1195  
 1196

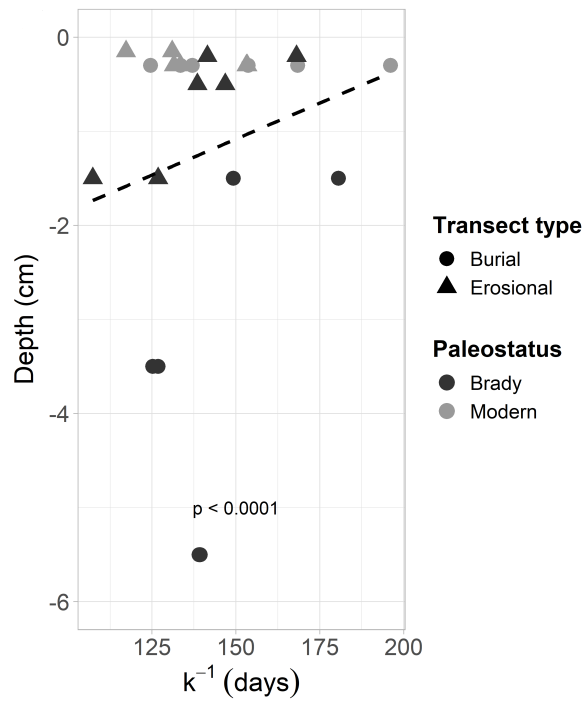


**Fig. 5** Decay constant of the slow cycling pool of modern and Brady soils at different depths (from the soil surface), incubated under wet-dry cycling conditions. Samples collected from burial and erosional transect types. Dotted line indicates exponential decay.

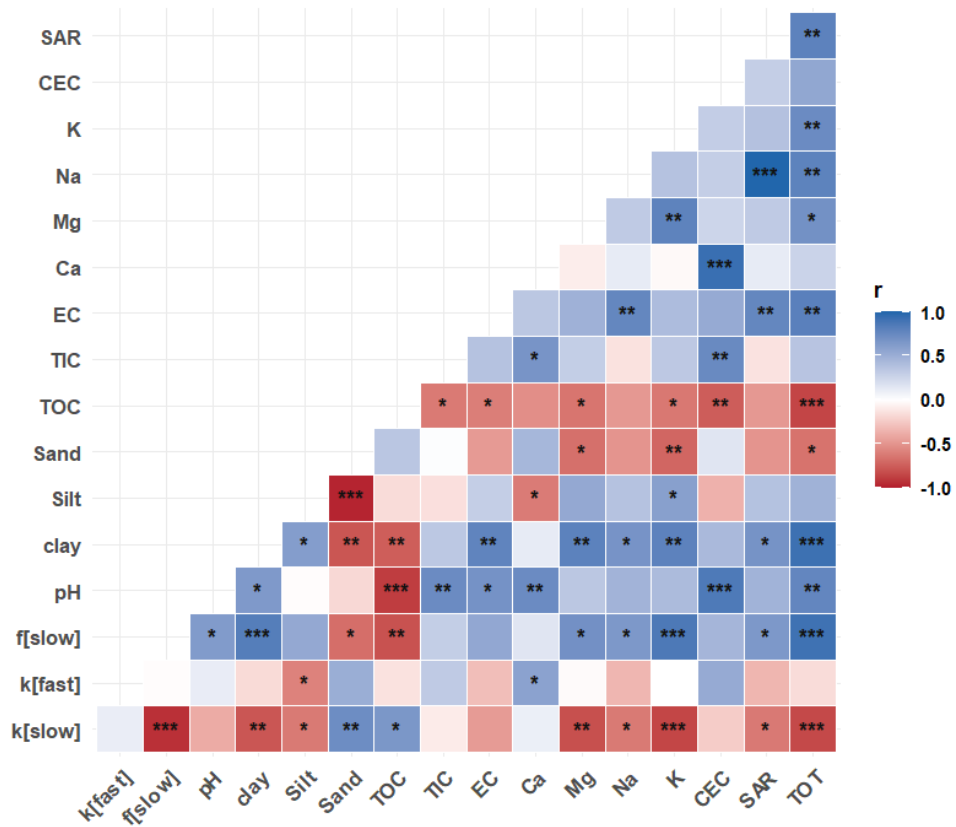


**Fig. 6** Correlation between soil physicochemical properties and modeled soil organic matter decomposition parameters (decay constant, k, and fraction of C in slow pool, f) for fast- and slow-cycling pools in modern and Brady soils incubated under continuously wet conditions. Decomposition parameters were obtained by multiple linear regression across burial and erosional transects. The statistical significance of each correlation is denoted by asterisks (\*\*\* for  $p < 0.001$ , \*\* for  $p < 0.01$ , \* for  $p < 0.05$ ).

1243  
1244  
1245  
1246  
1247  
1248  
1249  
1250  
1251  
1252  
1253  
1254  
1255  
1256  
1257  
1258  
1259  
1260  
1261  
1262  
1263  
1264  
1265  
1266  
1267  
1268  
1269  
1270  
1271  
1272  
1273  
1274  
1275  
1276  
1277  
1278  
1279  
1280  
1281  
1282  
1283  
1284  
1285  
1286  
1287  
1288

**Table 1** General physicochemical (mean  $\pm$  standard deviation) of soils used in the incubation experiment, grouped by transect type and paleostatus

<b>Transect type</b> <b>Paleostatus</b>	Burial		Erosional	
	Brady	Modern	Brady	Modern
pH	7.77 $\pm$ 0.04	6.89 $\pm$ 0.32	7.68 $\pm$ 0.12	7.41 $\pm$ 0.10
Clay (%)	9.48 $\pm$ 0.75	6.13 $\pm$ 0.64	7.62 $\pm$ 0.44	6.29 $\pm$ 0.48
Silt (%)	59.31 $\pm$ 0.44	56.24 $\pm$ 5.76	55.73 $\pm$ 4.88	53.67 $\pm$ 1.51
Sand (%)	31.24 $\pm$ 0.94	37.62 $\pm$ 6.39	36.64 $\pm$ 5.22	40.08 $\pm$ 1.92
TOC content	0.45 $\pm$ 0.06	1.03 $\pm$ 0.20	0.56 $\pm$ 0.10	0.93 $\pm$ 0.17
TIC content	0.24 $\pm$ 0.11	0.09 $\pm$ 0.03	0.28 $\pm$ 0.04	0.25 $\pm$ 0.03
EC (dS m <sup>-1</sup> )	5.41 $\pm$ 0.32	2.26 $\pm$ 0.43	3.05 $\pm$ 0.47	3.57 $\pm$ 0.35
CEC (cmolc kg <sup>-1</sup> )	22.86 $\pm$ 0.54	15.17 $\pm$ 3.54	23.31 $\pm$ 3.52	20.59 $\pm$ 1.83
Turnover time (y)	15654 $\pm$ 2440	576.4 $\pm$ 126	8327 $\pm$ 2732	1451 $\pm$ 673
CN ratio	10.00 $\pm$ 0.45	9.24 $\pm$ 0.21	10.96 $\pm$ 0.20	9.76 $\pm$ 0.25

1289  
1290  
1291  
1292  
1293  
1294  
1295  
1296  
1297  
1298  
1299  
1300  
1301  
1302  
1303  
1304  
1305  
1306  
1307  
1308  
1309  
1310  
1311  
1312  
1313  
1314  
1315  
1316  
1317  
1318  
1319  
1320  
1321  
1322  
1323  
1324  
1325  
1326  
1327  
1328  
1329  
1330  
1331  
1332  
1333  
1334

**Table 2** Soil organic matter (SOM) decomposition parameters (decay rate  $k$  of one-pool model, decay rates of fast- ( $k_{\text{fast}}$ ) and slow-cycling ( $k_{\text{slow}}$ ) SOM pools, and fraction sizes of fast ( $f_{\text{fast}}$ ) and slow ( $f_{\text{slow}}$ ) pools, grouped by experiment, transect type, and paleostatus.

Experiment	CW				WD			
	Burial		Erosional		Burial		Erosional	
Transect type	Brady	Modern	Brady	Modern	Brady	Modern	Brady	Modern
Paleostatus	Brady	Modern	Brady	Modern	Brady	Modern	Brady	Modern
$k$ (one pool)	0.0107	0.0099	0.0069	0.0072	0.0071	0.0067	0.0074	0.0074
$k_{\text{slow}}$	<0.0001	<0.0001	<0.0001	<0.0001	0.0080	0.0074	0.0086	0.0084
$k_{\text{fast}}$	0.1250	0.1264	0.1333	0.1270	6.6931	6.3419	0.4222	9.8728
$f_{\text{slow}}$	0.9920	0.9836	0.9903	0.9818	0.9990	0.9990	0.9990	0.9990
$f_{\text{fast}}$	0.0080	0.0164	0.0097	0.0182	0.0010	0.0010	0.0010	0.0010

1335  
1336  
1337  
1338  
1339  
1340  
1341  
1342  
1343  
1344  
1345  
1346  
1347  
1348  
1349  
1350  
1351  
1352  
1353  
1354  
1355  
1356  
1357  
1358  
1359  
1360  
1361  
1362  
1363  
1364  
1365  
1366  
1367  
1368  
1369  
1370  
1371  
1372  
1373  
1374  
1375  
1376  
1377  
1378  
1379  
1380

**Table 3** Summary of multiple linear regression models showing key positive (+) and negative (-) predictors of model parameters (proportions of fast and slow cycling fractions of TOC, i.e.,  $f_f$  and  $f_s$  and the corresponding decay rate constants  $k_f$  and  $k_s$ ), model performance ( $R^2$ ), and root mean square error (RMSE).

Model parameter	Key (+) predictors	Key (-) predictors	$R^2$	RMSE
$k_{slow}$	clay, Ca, EC	SAR, Mg, K, pH, TOC, TIC	0.98	$7.01 \times 10^{-7}$
$k_{fast}$	SAR, clay, Ca, Mg, TIC	K, EC, pH	0.95	$1.41 \times 10^{-3}$
$f_{slow}$	SAR, Mg, K, pH, TIC	clay, Ca, EC, TOC	0.97	$8.38 \times 10^{-4}$
$f_{fast}$	clay, Ca, EC, TOC	SAR, Mg, K, pH, TIC	0.97	$8.38 \times 10^{-4}$
$k_{one-pool}$	clay, K, pH, TOC	SAR, Ca, Mg	0.94	$2.15 \times 10^{-4}$

## Appendix A

1381  
1382  
1383  
1384  
1385  
1386  
1387  
1388  
1389  
1390  
1391  
1392  
1393  
1394  
1395  
1396  
1397  
1398  
1399  
1400  
1401  
1402  
1403  
1404  
1405  
1406  
1407  
1408  
1409  
1410  
1411  
1412  
1413  
1414  
1415  
1416  
1417  
1418  
1419  
1420  
1421  
1422  
1423  
1424  
1425  
1426

1427  
 1428  
 1429  
 1430  
 1431  
 1432  
 1433  
 1434  
 1435  
 1436  
 1437  
 1438  
 1439  
 1440  
 1441  
 1442  
 1443  
 1444  
 1445  
 1446  
 1447  
 1448  
 1449  
 1450  
 1451  
 1452  
 1453  
 1454  
 1455  
 1456  
 1457  
 1458  
 1459  
 1460  
 1461  
 1462  
 1463  
 1464  
 1465  
 1466  
 1467  
 1468  
 1469  
 1470  
 1471  
 1472

**Table A1** Absolute sampling depth intervals i.e., depth from soil surface (standard deviation in brackets for  $n = 3$ ) of modern (surface) and Brady (burial) soils along two types of transects, where degrees of burial or exposure increase from degrees I to III. Table adapted from [Dohui et al. \(2026b\)](#)

Depth (cm)	Transect Type					
	Erosional		Degree		Burial	
	III	II	I	I	II	III
Modern	0-19 (2.5)	0-19 (3.2)	0-18 (3.5)	0-30 (0.6)	0-29 (0.6)	0-29 (0.0)
Paleostatus	NA	19-38 (3.6)	18-36 (3.5)	30-60 (0.6)	29-59 (2.3)	29-59 (2.3)
	20-50 (1.2)	50-80 (0.0)	150-180 (0.0)	100-130 (4.0)	300-330 (9.3)	550-580 (6.7)
Brady	50-80 (0.4)	80-120 (0.0)	180-210 (2.9)	130-160 (4.5)	330-360 (2.6)	580-610 (5.6)

1473  
 1474  
 1475  
 1476  
 1477  
 1478  
 1479  
 1480  
 1481  
 1482  
 1483  
 1484  
 1485  
 1486  
 1487  
 1488  
 1489  
 1490  
 1491  
 1492  
 1493  
 1494  
 1495  
 1496  
 1497  
 1498  
 1499  
 1500  
 1501  
 1502  
 1503  
 1504  
 1505  
 1506  
 1507  
 1508  
 1509  
 1510  
 1511  
 1512  
 1513  
 1514  
 1515  
 1516  
 1517  
 1518

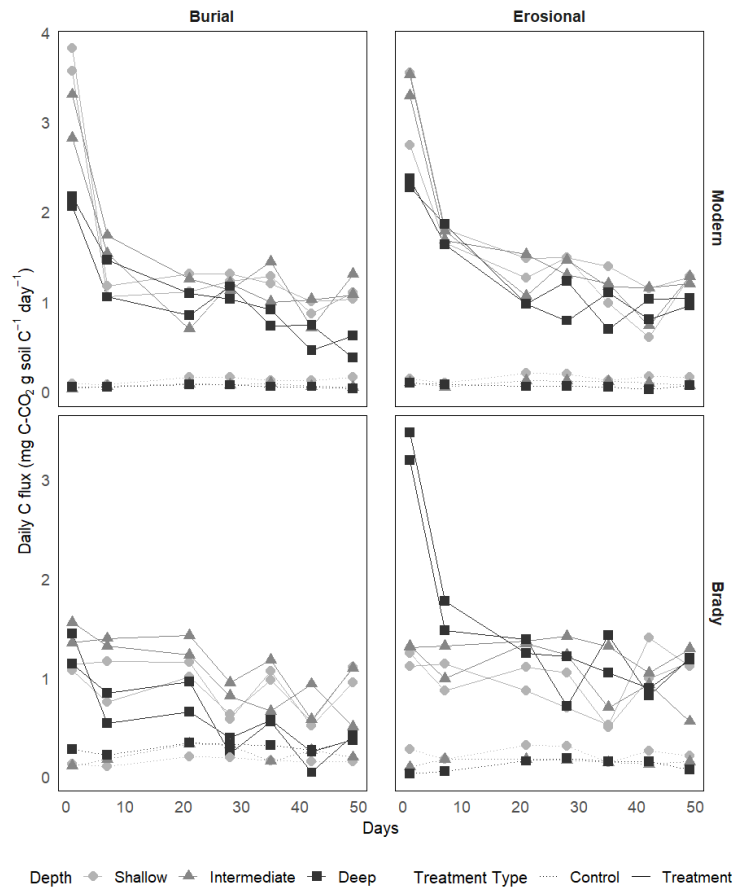


**Fig. A1** Daily respiratory CO<sub>2</sub> flux from modern and Brady Soil sampled from three depths representing varying degrees of burial/erosional exposure (two technical replicates each). In burial transects, Shallow → Intermediate → Deep corresponds to burial degrees I → II → III. In erosional transects, this relationship is reversed, with Shallow → Intermediate → Deep corresponding to exposure degrees III → II → I. Soils were wetted to a moisture content of 60% water holding capacity (WHC) and allowed to dry to 5% WHC. The dotted line represents the control (constant 5% WHC).

1519  
 1520  
 1521  
 1522  
 1523  
 1524  
 1525  
 1526  
 1527  
 1528  
 1529  
 1530  
 1531  
 1532  
 1533  
 1534  
 1535  
 1536  
 1537  
 1538  
 1539  
 1540  
 1541  
 1542  
 1543  
 1544  
 1545  
 1546  
 1547  
 1548  
 1549  
 1550  
 1551  
 1552  
 1553  
 1554  
 1555  
 1556  
 1557  
 1558  
 1559  
 1560  
 1561  
 1562  
 1563  
 1564

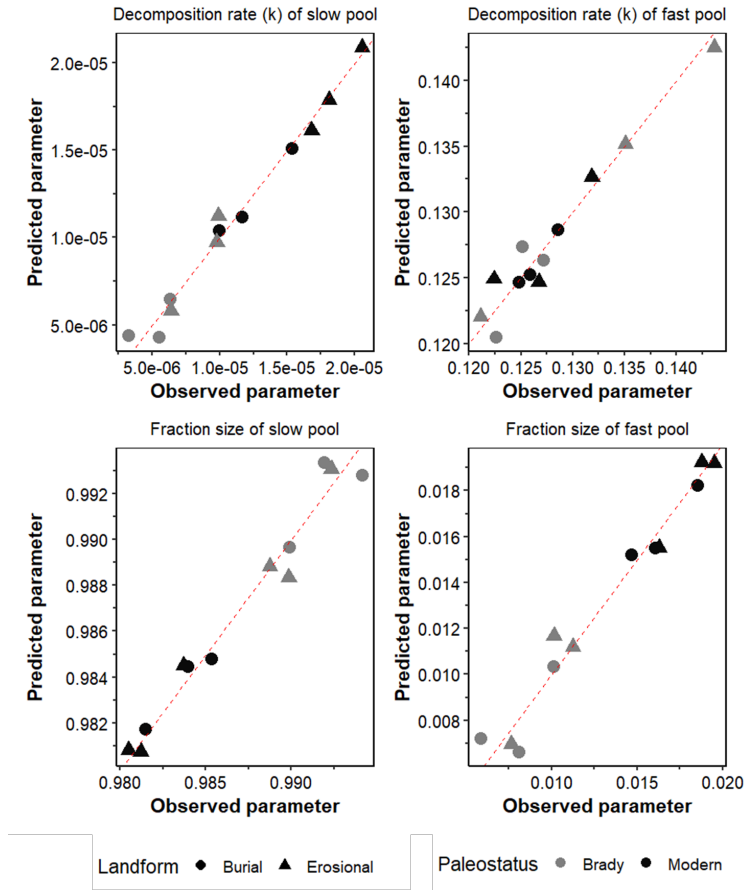


**Fig. A2** True versus predicted soil organic matter decomposition parameters (decay constant,  $k$ , and fraction of C in slow pool,  $f$ ) for fast- and slow-cycling pools in modern and Brady soils incubated under continuously wet conditions. These parameters were obtained by multiple linear regression across burial and erosional transects. Red dotted line represents  $y = x$ .

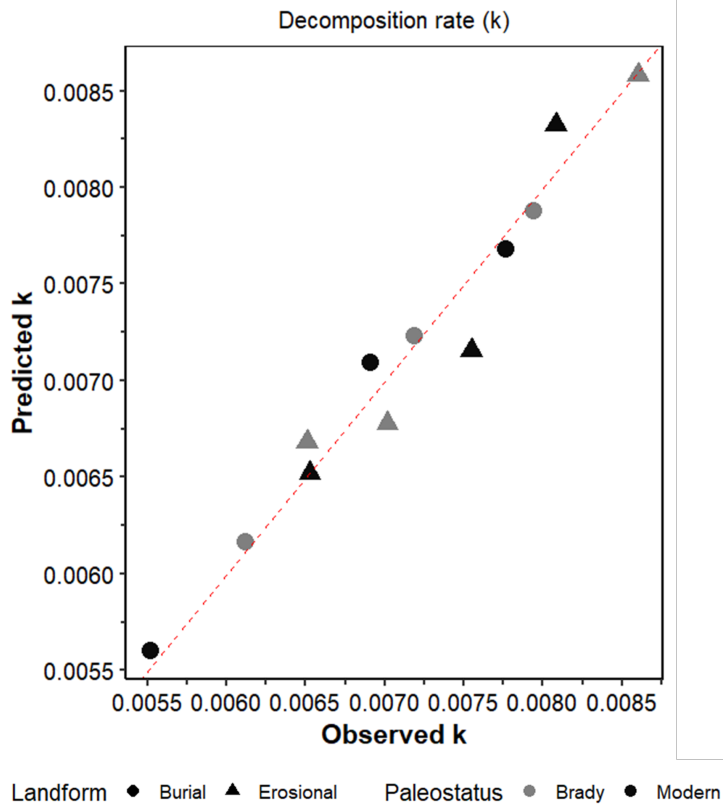


**Fig. A3** True versus predicted soil organic matter decay constant,  $k$  in modern and Brady soils incubated under wet-dry cycling conditions. These parameters were obtained by multiple linear regression across burial and erosional transects. Red dotted line represents  $y = x$ .

1565  
 1566  
 1567  
 1568  
 1569  
 1570  
 1571  
 1572  
 1573  
 1574  
 1575  
 1576  
 1577  
 1578  
 1579  
 1580  
 1581  
 1582  
 1583  
 1584  
 1585  
 1586  
 1587  
 1588  
 1589  
 1590  
 1591  
 1592  
 1593  
 1594  
 1595  
 1596  
 1597  
 1598  
 1599  
 1600  
 1601  
 1602  
 1603  
 1604  
 1605  
 1606  
 1607  
 1608  
 1609  
 1610

1611  
 1612  
 1613  
 1614  
 1615  
 1616  
 1617  
 1618  
 1619  
 1620  
 1621  
 1622  
 1623  
 1624  
 1625  
 1626  
 1627  
 1628  
 1629  
 1630  
 1631  
 1632  
 1633  
 1634  
 1635  
 1636  
 1637  
 1638  
 1639  
 1640  
 1641  
 1642  
 1643  
 1644  
 1645  
 1646  
 1647  
 1648  
 1649  
 1650  
 1651  
 1652  
 1653  
 1654  
 1655  
 1656

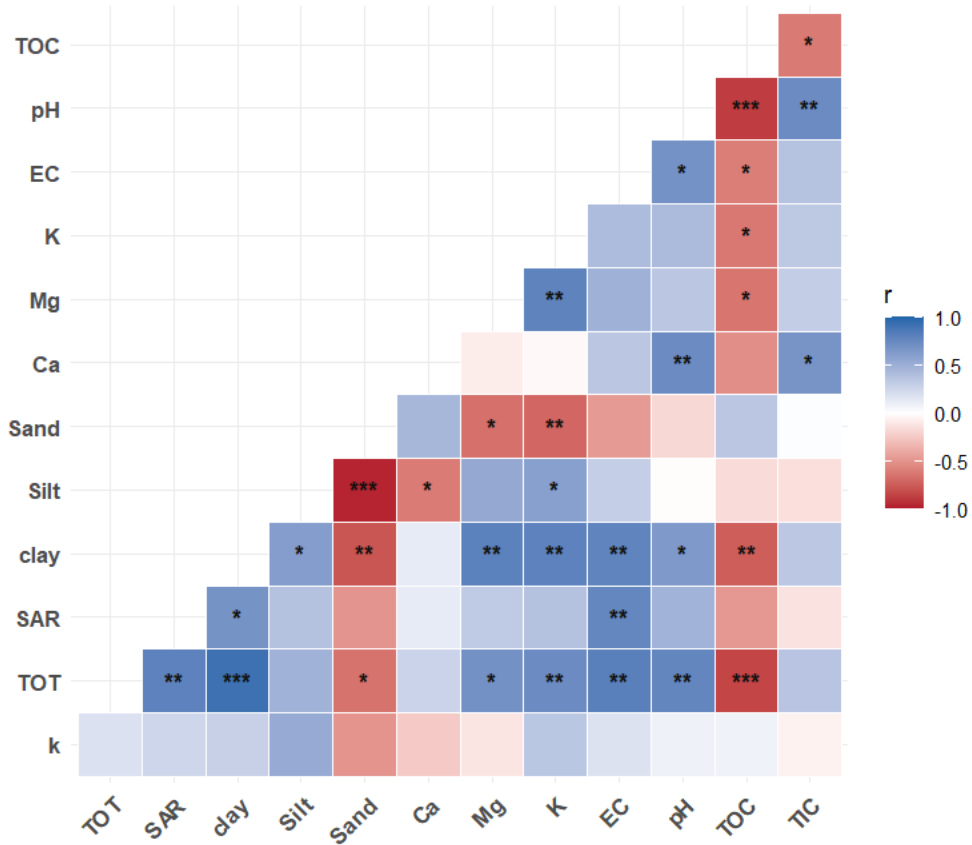


**Fig. A4** Correlation between soil physicochemical properties and modeled soil organic matter decomposition parameters (decay constant, k, and fraction of C in slow pool, f) for fast- and slow-cycling pools in modern and Brady soils incubated under wet-dry cycles. Decomposition parameters were obtained by multiple linear regression across burial and erosional transects. The statistical significance of each correlation is denoted by asterisks (\*\*\* for  $p < 0.001$ , \*\* for  $p < 0.01$ , \* for  $p < 0.05$ ).

## A.1 Multiple linear regression equations

$$\begin{aligned} k_{slow} = & 0.0000532 - 0.0000979 \cdot SAR + 0.00000225 \cdot clay + 0.000000395 \cdot Ca \\ & - 0.00000622 \cdot Mg - 0.00000271 \cdot K + 0.00000347 \cdot EC - 0.00000618 \cdot pH \\ & - 0.00000687 \cdot TOC - 0.0000275 \cdot TIC \end{aligned} \quad (A1)$$

$$RMSE : 0.000000701, \quad R^2 : 0.98$$

$$\begin{aligned} k_{fast} = & 0.215 + 0.0189 \cdot SAR + 0.00344 \cdot clay + 0.0026 \cdot Ca + 0.00204 \cdot Mg \\ & - 0.000302 \cdot K - 0.00513 \cdot EC - 0.0196 \cdot pH + 0.0146 \cdot TIC \end{aligned} \quad (A2)$$

$$RMSE : 0.00141, \quad R^2 : 0.95$$

$$\begin{aligned} f_{slow} = & 0.976 + 0.0732 \cdot SAR - 0.000362 \cdot clay - 0.000241 \cdot Ca + 0.00138 \cdot Mg \\ & + 0.00283 \cdot K - 0.00288 \cdot EC + 0.00174 \cdot pH - 0.000707 \cdot TOC \\ & + 0.0298 \cdot TIC \end{aligned} \quad (A3)$$

$$RMSE : 0.000838, \quad R^2 : 0.97$$

$$\begin{aligned} f_{fast} = & 0.0243 - 0.0732 \cdot SAR + 0.000362 \cdot clay + 0.000241 \cdot Ca - 0.00138 \cdot Mg \\ & - 0.00283 \cdot K + 0.00288 \cdot EC - 0.00174 \cdot pH + 0.000707 \cdot TOC \\ & - 0.0298 \cdot TIC \end{aligned}$$

$$RMSE : 0.000838, \quad R^2 : 0.97$$

(A4)

$$\begin{aligned} k(one - pool) = & -0.00641 - 0.00308 \cdot SAR + 0.000599 \cdot clay - 0.000141 \cdot Ca \\ & - 0.0015 \cdot Mg + 0.00118 \cdot K + 0.00159 \cdot pH \\ & + 0.002 \cdot TOC \end{aligned} \quad (A5)$$

$$RMSE : 0.000215, \quad R^2 : 0.94$$

## References

Batool M, Cihacek LJ, Alghamdi RS (2024) Soil Inorganic Carbon Formation and the Sequestration of Secondary Carbonates in Global Carbon Pools: A Review. *Soil Systems* 8(1):15. <https://doi.org/10.3390/soilsystems8010015>

Beare M, Gregorich E, St-Georges P (2009) Compaction effects on CO<sub>2</sub> and N<sub>2</sub>O production during drying and rewetting of soil. *Soil Biology and Biochemistry* 41(3):611–621. <https://doi.org/10.1016/j.soilbio.2008.12.024>

1703 Berhe AA, Harte J, Harden JW, Torn MS (2007) The Significance of the Erosion-  
1704 induced Terrestrial Carbon Sink. *BioScience* 57(4):337–346. [https://doi.org/10.](https://doi.org/10.1641/B570408)  
1705 [1641/B570408](https://doi.org/10.1641/B570408)  
1706  
1707 Berhe AA, Harden JW, Torn MS, Harte J (2008) Linking soil organic matter dynamics  
1708 and erosion-induced terrestrial carbon sequestration at different landform positions.  
1709 *Journal of Geophysical Research: Biogeosciences* 113(G4). [https://doi.org/10.1029/](https://doi.org/10.1029/2008JG000751)  
1710 [2008JG000751](https://doi.org/10.1029/2008JG000751)  
1711  
1712 Berhe AA, Suttle KB, Burton SD, Banfield JF (2012) Contingency in the direction  
1713 and mechanics of soil organic matter responses to increased rainfall. *Plant and Soil*  
1714 358(1-2):371–383. <https://doi.org/10.1007/s11104-012-1156-0>  
1715  
1716 Berhe AA, Barnes RT, Six J, Marín-Spiotta E (2018) Role of Soil Erosion in Biogeo-  
1717 chemical Cycling of Essential Elements: Carbon, Nitrogen, and Phosphorus. *Annual*  
1718 *Review of Earth and Planetary Sciences* 46(1):521–548. [https://doi.org/10.1146/](https://doi.org/10.1146/annurev-earth-082517-010018)  
1719 [annurev-earth-082517-010018](https://doi.org/10.1146/annurev-earth-082517-010018)  
1720  
1721 Bird JA, Torn MS (2006) Fine Roots vs. Needles: A Comparison of <sup>13</sup>C and <sup>15</sup>N  
1722 Dynamics in a Ponderosa Pine Forest Soil. *Biogeochemistry* 79(3):361–382. <https://doi.org/10.1007/s10533-005-5632-y>  
1723  
1724 Chaopricha NT (2013) The Importance, Origin, Composition, and Stability of Deeply  
1725 Buried Soil Organic Matter. PhD thesis, University of Wisconsin-Madison, Madison  
1726  
1727 Chaopricha NT, Marín-Spiotta E (2014) Soil burial contributes to deep soil organic  
1728 carbon storage. *Soil Biology and Biochemistry* 69:251–264. [https://doi.org/10.1016/](https://doi.org/10.1016/j.soilbio.2013.11.011)  
1729 [j.soilbio.2013.11.011](https://doi.org/10.1016/j.soilbio.2013.11.011)  
1730  
1731 Chowdhury N, Marschner P, Burns RG (2011) Soil microbial activity and community  
1732 composition: Impact of changes in matric and osmotic potential. *Soil Biology and*  
1733 *Biochemistry* 43(6):1229–1236. <https://doi.org/10.1016/j.soilbio.2011.02.012>  
1734  
1735 Cotrufo MF, Lavelle JM (2025) Incorporating aridity in soil carbon steward-  
1736 ship frameworks. *Nature Climate Change* 15(3):240–242. [https://doi.org/10.1038/](https://doi.org/10.1038/s41558-025-02270-9)  
1737 [s41558-025-02270-9](https://doi.org/10.1038/s41558-025-02270-9)  
1738  
1739 Davidson EA, Samanta S, Caramori SS, Savage K (2012) The  $k_{D_i}/k_{A_i}$  and  $k_{M_i}/k_{M_j}$  Michaelis–Menten kinetics model  
1740 for decomposition of soil organic matter at hourly to seasonal time scales. *Global*  
1741 *Change Biology* 18(1):371–384. <https://doi.org/10.1111/j.1365-2486.2011.02546.x>  
1742  
1743 Dolui M, Nel T, Chacon S, Phillips LM, McMurtry AR, Moreland K, McFarlane  
1744 K, Mason JA, Marín-Spiotta E, de Graaff M, Ghezzehei T, Berhe AA (2026a)  
1745 Soil Organic Matter Stabilization by Polyvalent Cations in a Buried Alkaline Soil.  
1746 *Journal of Geophysical Research: Biogeosciences* 131(2). [https://doi.org/10.1029/](https://doi.org/10.1029/2025JG009241)  
1747 [2025JG009241](https://doi.org/10.1029/2025JG009241)  
1748

Dolui M, Nel T, Phillips LM, McMurtry AR, Moreland K, Tfaily M, McFarlane K, Mason JA, Marin-Spiotta E, de Graaff MA, Ghezzehei T, Berhe AA (2026b) Composition and persistence of soil organic matter along eroding and depositional transects in buried vs. modern soil layers: A case of the Brady paleosol at Wauneta, Nebraska. *Geoderma* 465:117660. <https://doi.org/10.1016/j.geoderma.2025.117660>

Elzhov T, Mullen K, Spiess A, Bolker B (2023) minpack.lm: R Interface to the Levenberg-Marquardt Nonlinear Least-Squares Algorithm Found in MINPACK, Plus Support for Bounds. URL <https://CRAN.R-project.org/package=minpack.lm>.

Fierer N, Schimel JP (2003) A Proposed Mechanism for the Pulse in Carbon Dioxide Production Commonly Observed Following the Rapid Rewetting of a Dry Soil. *Soil Science Society of America Journal* 67(3):798. <https://doi.org/10.2136/sssaj2003.0798>

Fontaine S, Barot S, Barré P, Bdioui N, Mary B, Rumpel C (2007) Stability of organic carbon in deep soil layers controlled by fresh carbon supply. *Nature* 450(7167):277–280. <https://doi.org/10.1038/nature06275>

Gao X, Huang R, Li J, Wang C, Lan T, Li Q, Deng O, Tao Q, Zeng M (2020) Temperature induces soil organic carbon mineralization in urban park green spaces, Chengdu, southwestern China: Effects of planting years and vegetation types. *Urban Forestry & Urban Greening* 54:126761. <https://doi.org/10.1016/j.ufug.2020.126761>

Ghezzehei TA, Sulman B, Arnold CL, Bogie NA, Berhe AA (2019) On the role of soil water retention characteristic on aerobic microbial respiration. *Biogeosciences* 16(6):1187–1209. <https://doi.org/10.5194/bg-16-1187-2019>

Goebel MO, Bachmann J, Woche SK, Fischer WR (2005) Soil wettability, aggregate stability, and the decomposition of soil organic matter. *Geoderma* 128(1-2):80–93. <https://doi.org/10.1016/j.geoderma.2004.12.016>

Griffiths BS, Philippot L (2013) Insights into the resistance and resilience of the soil microbial community. *FEMS Microbiology Reviews* 37(2):112–129. <https://doi.org/10.1111/j.1574-6976.2012.00343.x>

Hicks Pries CE, Castanha C, Porras RC, Torn MS (2017) The whole-soil carbon flux in response to warming. *Science* 355(6332):1420–1423. <https://doi.org/10.1126/science.aal1319>

Hicks Pries CE, Ryals R, Zhu B, Min K, Cooper A, Goldsmith S, Pett-Ridge J, Torn M, Berhe AA (2023) The Deep Soil Organic Carbon Response to Global Change. *Annual Review of Ecology, Evolution, and Systematics* 54(1):375–401. <https://doi.org/10.1146/annurev-ecolsys-102320-085332>

Hill RL, Horton R, Cruse RM (1985) Tillage Effects on Soil Water Retention and Pore Size Distribution of Two Mollisols. *Soil Science Society of America Journal*

1795 49(5):1264–1270. <https://doi.org/10.2136/sssaj1985.03615995004900050039x>  
1796  
1797 Horne D, McIntosh J (2000) Hydrophobic compounds in sands in New  
1798 Zealand—extraction, characterisation and proposed mechanisms for repel-  
1799 lency expression. *Journal of Hydrology* 231-232:35–46. [https://doi.org/10.1016/S0022-1694\(00\)00181-5](https://doi.org/10.1016/S0022-1694(00)00181-5)  
1800  
1801 Hunter BD, Roering JJ, Silva LCR, Moreland KC (2024) Geomorphic controls on  
1802 the abundance and persistence of soil organic carbon pools in erosional landscapes.  
1803 *Nature Geoscience* 17(2):151–157. <https://doi.org/10.1038/s41561-023-01365-2>  
1804  
1805 IPCC (2018) Global Warming of 1.5°C. In: Masson-Delmotte V, Zhai P, Pörtner  
1806 HO, Roberts D, Skea J, Shukla P, Pirani A, Moufouma-Okia W, Péan C, Pid-  
1807 cock R, Connors S, Matthews J, Chen Y, Zhou X, Gomis M, Lonnoy E, Maycock  
1808 T, Tignor M, Waterfield T (eds) An IPCC Special Report on the impacts of  
1809 global warming of 1.5°C above pre-industrial levels and related global green-  
1810 house gas emission pathways, in the context of strengthening the global response  
1811 to the threat of climate change. Intergovernmental Panel on Climate Change.,  
1812 <https://doi.org/10.1038/291285a0>  
1813  
1814 Jacobs PM, Mason JA (2004) Paleopedology of soils in thick Holocene loess, Nebraska,  
1815 USA. *Revista Mexicana de Ciencias Geológicas* 21(1):54–70  
1816  
1817 Jacobs PM, Mason JA (2007) Late Quaternary climate change, loess sedimentation,  
1818 and soil profile development in the central Great Plains: A pedosedimentary model.  
1819 *Geological Society of America Bulletin* 119(3-4):462–475. <https://doi.org/10.1130/B25868.1>  
1820  
1821  
1822 Jobbagy EG, Jackson RB (2000) The Vertical Distribution of Soil Organic Carbon  
1823 and Its Relation to Climate and Vegetation. *Ecological Applications* 10(2):423–436  
1824  
1825 Johnson WC, Willey KL (2000) Isotopic and rock magnetic expression of environ-  
1826 mental change at the Pleistocene–Holocene transition in the central Great Plains.  
1827 *Quaternary International* 67(1):89–106. [https://doi.org/10.1016/S1040-6182\(00\)](https://doi.org/10.1016/S1040-6182(00)00011-2)  
1828 [00011-2](https://doi.org/10.1016/S1040-6182(00)00011-2)  
1829  
1830 Johnson WC, Willey KL, Mason JA, May DW (2007) Stratigraphy and environmental  
1831 reconstruction at the middle Wisconsinan Gilman Canyon formation type locality,  
1832 Buzzard’s Roost, southwestern Nebraska, USA. *Quaternary Research* 67(3):474–  
1833 486. <https://doi.org/10.1016/j.yqres.2007.01.011>  
1834  
1835 Kaiser M, Kleber M, Berhe AA (2015) How air-drying and rewetting modify soil  
1836 organic matter characteristics: An assessment to improve data interpretation and  
1837 inference. *Soil Biology and Biochemistry* 80:324–340. [https://doi.org/10.1016/j.](https://doi.org/10.1016/j.soilbio.2014.10.018)  
1838 [soilbio.2014.10.018](https://doi.org/10.1016/j.soilbio.2014.10.018)  
1839  
1840

Kang S, Xing B (2008) Humic Acid Fractionation upon Sequential Adsorption onto Goethite. *Langmuir* 24(6):2525–2531. <https://doi.org/10.1021/la702914q> 1841  
1842  
1843

Kemper WD, Rosenau RC, Dexter AR (1987) Cohesion Development in Disrupted Soils as Affected by Clay and Organic Matter Content and Temperature. *Soil Science Society of America Journal* 51(4):860–867. <https://doi.org/10.2136/sssaj1987.03615995005100040004x> 1844  
1845  
1846  
1847  
1848

Lawrence CR, Harden JW, Xu X, Schulz MS, Trumbore SE (2015) Long-term controls on soil organic carbon with depth and time: A case study from the Cowlitz River Chronosequence, WA USA. *Geoderma* 247-248:73–87. <https://doi.org/10.1016/j.geoderma.2015.02.005> 1849  
1850  
1851  
1852  
1853

Lawrence CR, Schulz MS, Masiello CA, Chadwick OA, Harden JW (2021) The trajectory of soil development and its relationship to soil carbon dynamics. *Geoderma* 403:115378. <https://doi.org/10.1016/j.geoderma.2021.115378> 1854  
1855  
1856  
1857

Leizeaga A, Hicks LC, Manoharan L, Hawkes CV, Rousk J (2021) Drought legacy affects microbial community trait distributions related to moisture along a savannah grassland precipitation gradient. *Journal of Ecology* 109(9):3195–3210. <https://doi.org/10.1111/1365-2745.13550> 1858  
1859  
1860  
1861

Lenth RV (2024) emmeans: Estimated Marginal Means, aka Least-Squares Means. URL <https://CRAN.R-project.org/package=emmeans> 1862  
1863  
1864

Li Q, Hu W, Li L, Li Y (2023) Interactions between organic matter and Fe oxides at soil micro-interfaces: Quantification, associations, and influencing factors. *Science of The Total Environment* 855:158710. <https://doi.org/10.1016/j.scitotenv.2022.158710> 1865  
1866  
1867  
1868

Liu T, Wang L, Feng X, Zhang J, Ma T, Wang X, Liu Z (2018) Comparing soil carbon loss through respiration and leaching under extreme precipitation events in arid and semiarid grasslands. *Biogeosciences* 15(5):1627–1641. <https://doi.org/10.5194/bg-15-1627-2018> 1869  
1870  
1871  
1872  
1873

Marin-Spiotta E, Chadwick OA, Kramer M, Carbone MS (2011) Carbon delivery to deep mineral horizons in Hawaiian rain forest soils. *Journal of Geophysical Research* 116(G3):G03011. <https://doi.org/10.1029/2010JG001587> 1874  
1875  
1876  
1877

Marin-Spiotta E, Chaopricha NT, Plante AF, Diefendorf AF, Mueller CW, Grandy AS, Mason JA (2014) Long-term stabilization of deep soil carbon by fire and burial during early Holocene climate change. *Nature Geoscience* 7(6):428–432. <https://doi.org/10.1038/ngeo2169> 1878  
1879  
1880  
1881

Mason JA, Jacobs PM, Hanson PR, Miao X, Goble RJ (2003) Sources and paleoclimatic significance of Holocene Bignell Loess, central Great Plains, USA. *Quaternary Research* 60(3):330–339. <https://doi.org/10.1016/j.yqres.2003.07.005> 1882  
1883  
1884  
1885  
1886

1887 Mason JA, Miao X, Hanson PR, Johnson WC, Jacobs PM, Goble RJ (2008) Loess  
 1888 record of the Pleistocene–Holocene transition on the northern and central Great  
 1889 Plains, USA. *Quaternary Science Reviews* 27(17-18):1772–1783. [https://doi.org/10.](https://doi.org/10.1016/j.quascirev.2008.07.004)  
 1890 [1016/j.quascirev.2008.07.004](https://doi.org/10.1016/j.quascirev.2008.07.004)  
 1891  
 1892 McDowell T (2020) Processes controlling soil hydrology and pedogenic carbon-  
 1893 ate formation in loess tablelands, Nebraska, USA. PhD thesis, University of  
 1894 Wisconsin-Madison, Madison  
 1895  
 1896 McDowell TM, Mason JA, Vo T, Marin-Spiotta E (2022) Hydrology of a Semi-  
 1897 arid Loess-Paleosol Sequence, and Implications for Buried Soil Connection to  
 1898 the Modern Climate, Plant-Available Moisture, and Loess Tableland Persistence.  
 1899 *Journal of Geophysical Research: Earth Surface* 127(12). [https://doi.org/10.1029/](https://doi.org/10.1029/2022JF006800)  
 1900 [2022JF006800](https://doi.org/10.1029/2022JF006800)  
 1901  
 1902 McMurtry AR, Kasmerchak CS, Vaughan EA, Dolui M, Phillips LM, Mueller CW,  
 1903 Pett-Ridge J, Berhe AA, Mason JA, Marín-Spiotta E, de Graaff MA (2024) Getting  
 1904 to the root of the problem: Soil carbon and microbial responses to root inputs  
 1905 within a buried paleosol along an eroding hillslope in southwestern Nebraska, USA.  
 1906 *Soil Biology and Biochemistry* 198:109549. [https://doi.org/10.1016/j.soilbio.2024.](https://doi.org/10.1016/j.soilbio.2024.109549)  
 1907 [109549](https://doi.org/10.1016/j.soilbio.2024.109549)  
 1908  
 1909 Miao X, Mason JA, Swinehart JB, Loope DB, Hanson PR, Goble RJ, Liu X (2007) A  
 1910 10,000 year record of dune activity, dust storms, and severe drought in the central  
 1911 Great Plains. *Geology* 35(2):119. <https://doi.org/10.1130/G23133A.1>  
 1912  
 1913 Miller A, Schimel J, Meixner T, Sickman J, Melack J (2005) Episodic rewet-  
 1914 ting enhances carbon and nitrogen release from chaparral soils. *Soil Biology and*  
 1915 *Biochemistry* 37(12):2195–2204. <https://doi.org/10.1016/j.soilbio.2005.03.021>  
 1916  
 1917 Min K, Berhe AA, Khoi CM, van Asperen H, Gillabel J, Six J (2020) Differential  
 1918 effects of wetting and drying on soil CO<sub>2</sub> concentration and flux in near-surface  
 1919 vs. deep soil layers. *Biogeochemistry* 148(3):255–269. [https://doi.org/10.1007/](https://doi.org/10.1007/s10533-020-00658-7)  
 1920 [s10533-020-00658-7](https://doi.org/10.1007/s10533-020-00658-7)  
 1921  
 1922 Najera F, Dippold MA, Boy J, Seguel O, Koester M, Stock S, Merino C, Kuzyakov  
 1923 Y, Matus F (2020) Effects of drying/rewetting on soil aggregate dynamics and  
 1924 implications for organic matter turnover. *Biology and Fertility of Soils* 56(7):893–  
 1925 905. <https://doi.org/10.1007/s00374-020-01469-6>  
 1926  
 1927 Naorem A, Jayaraman S, Dalal RC, Patra A, Rao CS, Lal R (2022) Soil Inorganic Car-  
 1928 bon as a Potential Sink in Carbon Storage in Dryland Soils—A Review. *Agriculture*  
 1929 12(8):1256. <https://doi.org/10.3390/agriculture12081256>  
 1930  
 1931 Neff JC, Asner GP (2001) Dissolved Organic Carbon in Terrestrial Ecosystems: Syn-  
 1932 thesis and a Model. *Ecosystems* 4(1):29–48. <https://doi.org/10.1007/s100210000058>

Or D, Tuller M (1999) Liquid retention and interfacial area in variably saturated porous media: Upscaling from single-pore to sample-scale model. *Water Resources Research* 35(12):3591–3605. <https://doi.org/10.1029/1999WR900262>

Pal SC, Chakraborty R, Towfiqul Islam ARM, Roy P, Chowdhuri I, Saha A, Islam A, Costache R, Alam E (2023) Land use and climate change-induced soil erosion mapping in a sub-tropical environment. *Geomatics, Natural Hazards and Risk* 14(1). <https://doi.org/10.1080/19475705.2023.2270129>

Patton NR, Lohse KA, Seyfried MS, Godsey SE, Parsons SB (2019) Topographic controls of soil organic carbon on soil-mantled landscapes. *Scientific Reports* 9(1):6390. <https://doi.org/10.1038/s41598-019-42556-5>

Pausch J, Loeppmann S, Kühnel A, Forbush K, Kuzyakov Y, Cheng W (2016) Rhizosphere priming of barley with and without root hairs. *Soil Biology and Biochemistry* 100:74–82. <https://doi.org/10.1016/j.soilbio.2016.05.009>

Pinheiro J, Bates D, DebRoy S, Sarkar D, R Core Team (2024) nlme: Linear and Nonlinear Mixed Effects Models. URL <https://CRAN.R-project.org/package=nlme>

R Core Team (2025) R: A Language and Environment for Statistical Computing. URL <https://www.r-project.org/>

Rasmussen C, Heckman K, Wieder WR, Keiluweit M, Lawrence CR, Berhe AA, Blankinship JC, Crow SE, Druhan JL, Hicks Pries CE, Marin-Spiotta E, Plante AF, Schädel C, Schimel JP, Sierra CA, Thompson A, Wagai R (2018) Beyond clay: towards an improved set of variables for predicting soil organic matter content. *Biogeochemistry* 137(3):297–306. <https://doi.org/10.1007/s10533-018-0424-3>

RStudio Team (2019) RStudio: Integrated Development for R. RStudio. URL <http://www.rstudio.com/>

Rumpel C, Kögel-Knabner I (2011) Deep soil organic matter—a key but poorly understood component of terrestrial C cycle. *Plant and Soil* 338(1-2):143–158. <https://doi.org/10.1007/s11104-010-0391-5>

Schmidt MWI, Torn MS, Abiven S, Dittmar T, Guggenberger G, Janssens IA, Kleber M, Kögel-Knabner I, Lehmann J, Manning DAC, Nannipieri P, Rasse DP, Weiner S, Trumbore SE (2011) Persistence of soil organic matter as an ecosystem property. *Nature* 478(7367):49–56. <https://doi.org/10.1038/nature10386>

Schrumpf M, Kaiser K, Guggenberger G, Persson T, Kögel-Knabner I, Schulze ED (2013) Storage and stability of organic carbon in soils as related to depth, occlusion within aggregates, and attachment to minerals. *Biogeosciences* 10(3):1675–1691. <https://doi.org/10.5194/bg-10-1675-2013>

1979 Shariffar A, Minasny B, Arrouays D, Bouillon L, Chevallier T, van Deventer P, Field  
 1980 DJ, Gomez C, Jang HJ, Jeon SH, Koch J, McBratney AB, Malone BP, Marchant  
 1981 BP, Martin MP, Monger C, Munera-Echeverri JL, Padarian J, Pfeiffer M, Richer-  
 1982 de Forges AC, Saby NP, Singh K, Song XD, Zamanian K, Zhang GL, van Zijl G  
 1983 (2023) Soil inorganic carbon, the other and equally important soil carbon pool:  
 1984 Distribution, controlling factors, and the impact of climate change. p 165–231, <https://doi.org/10.1016/bs.agron.2022.11.005>  
 1985  
 1986  
 1987 Six J, Conant R, Paul E, Paustian K (2002) Review: Stabilization Mechanisms of Soil  
 1988 Organic Matter: Implications for C-Saturation of Soils. *Plant and Soil* 241(2):155–  
 1989 176  
 1990  
 1991 Slessarev EW, Chadwick OA, Sokol NW, Nuccio EE, Pett-Ridge J (2022) Rock  
 1992 weathering controls the potential for soil carbon storage at a continental scale.  
 1993 *Biogeochemistry* 157(1):1–13. <https://doi.org/10.1007/s10533-021-00859-8>  
 1994  
 1995 Soong JL, Castanha C, Hicks Pries CE, Ofiti N, Porras RC, Riley WJ, Schmidt MW,  
 1996 Torn MS (2021) Five years of whole-soil warming led to loss of subsoil carbon stocks  
 1997 and increased CO<sub>2</sub> efflux. *Science Advances* 7(21). <https://doi.org/10.1126/sciadv.abd1343>  
 1998  
 1999 Stacy EM, Hart SC, Hunsaker CT, Johnson DW, Berhe AA (2015) Soil carbon  
 2000 and nitrogen erosion in forested catchments: implications for erosion-induced ter-  
 2001 restrial carbon sequestration. *Biogeosciences* 12(16):4861–4874. <https://doi.org/10.5194/bg-12-4861-2015>  
 2002  
 2003  
 2004 Steenwerth K, Jackson L, Calderon F, Scow K, Rolston D (2005) Response of  
 2005 microbial community composition and activity in agricultural and grassland soils  
 2006 after a simulated rainfall. *Soil Biology and Biochemistry* 37(12):2249–2262. <https://doi.org/10.1016/j.soilbio.2005.02.038>  
 2007  
 2008  
 2009 Szymanski LM (2021) Spatial Distribution and Long-Term Persistence of Ancient  
 2010 Carbon in Buried Soils and Its Vulnerability to Landscape Disturbance. PhD thesis,  
 2011 University of Wisconsin-Madison, Madison  
 2012  
 2013 Thaler EA, Larsen IJ, Yu Q (2021) The extent of soil loss across the US Corn Belt.  
 2014 *Proceedings of the National Academy of Sciences* 118(8). <https://doi.org/10.1073/pnas.1922375118>  
 2015  
 2016  
 2017 Tsy-pin M, Macpherson G (2012) The effect of precipitation events on inor-  
 2018 ganic carbon in soil and shallow groundwater, Konza Prairie LTER Site, NE  
 2019 Kansas, USA. *Applied Geochemistry* 27(12):2356–2369. <https://doi.org/10.1016/j.apgeochem.2012.07.008>  
 2020  
 2021 Venables WN, Ripley BD (2002) MASS (Modern Applied Statistics with S). URL  
 2022 <https://CRAN.R-project.org/package=MASS>  
 2023  
 2024

Wahab LM, Kim S, Berhe AA (2025) Carbon and Nitrogen Dynamics in Subsoils After 20 years of Added Precipitation in a Mediterranean Grassland. <a href="https://doi.org/10.5194/egusphere-2024-3607">https://doi.org/10.5194/egusphere-2024-3607</a>	2025 2026 2027 2028
Xiang SR, Doyle A, Holden PA, Schimel JP (2008) Drying and rewetting effects on C and N mineralization and microbial activity in surface and subsurface California grassland soils. <i>Soil Biology and Biochemistry</i> 40(9):2281–2289. <a href="https://doi.org/10.1016/j.soilbio.2008.05.004">https://doi.org/10.1016/j.soilbio.2008.05.004</a>	2029 2030 2031 2032 2033
Yoo K, Amundson R, Heimsath AM, Dietrich WE (2006) Spatial patterns of soil organic carbon on hillslopes: Integrating geomorphic processes and the biological C cycle. <i>Geoderma</i> 130(1-2):47–65. <a href="https://doi.org/10.1016/j.geoderma.2005.01.008">https://doi.org/10.1016/j.geoderma.2005.01.008</a>	2034 2035 2036 2037
Zhu B, Cheng W (2013) Impacts of drying–wetting cycles on rhizosphere respiration and soil organic matter decomposition. <i>Soil Biology and Biochemistry</i> 63:89–96. <a href="https://doi.org/10.1016/j.soilbio.2013.03.027">https://doi.org/10.1016/j.soilbio.2013.03.027</a>	2038 2039 2040 2041 2042 2043 2044 2045 2046 2047 2048 2049 2050 2051 2052 2053 2054 2055 2056 2057 2058 2059 2060 2061 2062 2063 2064 2065 2066 2067 2068 2069 2070